Image Cover Sheet

CLASSIFICATION	SYSTEM NUMBER
UNCLASSIFIED	127314

TITLE

DIGITAL QUADRATURE DEMODULATION FOR RADAR ESM APPLICATIONS

System Number:

Patron Number:

Requester:

Notes:

DSIS Use only:

Deliver to: JR

National Defence / Défense nationale

DIGITAL QUADRATURE DEMODULATION FOR RADAR ESM APPLICATIONS

by

Robert Inkol and Ron Saper

DEFENCE RESEARCH ESTABLISHMENT OTTAWA
TECHNICAL NOTE 92-10

Canada

May 1992
Ottawa

National Defence / Défense nationale

DIGITAL QUADRATURE DEMODULATION FOR RADAR ESM APPLICATIONS

by

Robert Inkol and Ron Saper
Radar ESM Section
Electronic Warfare Division

DEFENCE RESEARCH ESTABLISHMENT OTTAWA
TECHNICAL NOTE 92-10

PCN
011LB

May 1992
Ottawa

ABSTRACT

Techniques for digital in-phase and quadrature demodulation are investigated for application in Radar Electronic Support Measures (RESM) systems.

RÉSUMÉ

Des techniques de démodulation numérique en phase et en quadrature sont examinées pour l'application à des systèmes de mesures de soutien électroniques radar.

EXECUTIVE SUMMARY

The feasibility of using digital techniques for the coherent demodulation of wideband signals was investigated. Several different design approaches and analysis methods were considered. It was found that the processing requirements to achieve good accuracy for pulse and other wide-band signals can be minimized through appropriate choice of intermediate frequency, the use of half-band finite impulse response filters, and the application of decimation. This suggests that an application specific integrated circuit implementation of a digital coherent demodulator should have potential cost and performance advantages over existing analog approaches.

TABLE OF CONTENTS

LIST OF FIGURES

LIST OF TABLES

1.0 INTRODUCTION

Radar Electronic Support Measures (RESM) systems perform the functions of detecting, classifying and identifying radars in the signal environment. Existing systems have relied on relatively simple signal processing techniques to achieve real-time performance with available technology. Typically the received radar pulses are characterized by measurements of frequency, angle-of-arrival, pulse width, amplitude and time-of-arrival obtained using analog signal processing techniques. Additional processing, largely using rule-based algorithms, sorts trains of pulses from individual radars, extracts additional information such as scan-pattern and pulse repetition interval, and attempts to classify and identify the radars. With modern radars showing a definite trend towards more complex behaviour such as frequency or pulse repetition interval agility and frequency or phase modulation, the limitations of this approach are becoming apparent. Consequently future RESM receivers must become much more sophisticated in extracting additional information from the signals to minimize the likelihood of ambiguous or erroneous results.

Technology advances including the availability of high-performance flash analog-to-digital (A/D) converters, digital signal processors and application specific integrated circuits, permit the replacement of many analog signal processing components and subsystems with digital signal processing techniques. Aside from achieving better stability and repeatability, more sophisticated algorithms can be implemented to improve the measurement of current signal parameters and to provide additional signal parameters.

Coherent quadrature demodulation is of particular interest. The removal of the carrier facilitates signal processing operations such as correlation. Phase can be directly extracted and optimal algorithms for frequency and amplitude demodulation can be implemented[1].

Coherent quadrature demodulation has been proven in radar systems which use within-pulse information for subsequent processing. Examples are MTI and look-down radars which use Doppler processing to reject clutter, synthetic aperture radars which do coherent processing to improve azimuth resolution, and coded pulse radars which use modulation internal to the pulse to achieve improved range resolution[2].

Phase information is of potential value in RESM systems. It has been proposed that a good way of characterizing signals having linear or non-linear frequency modulation is to fit a low-order polynomial to the unwrapped phase using the method of least squares[3]. A recently proposed approach for comparing pairs of time-aligned signals is based on the computation of the mean square error of their differential phase relative to an appropriate mathematical model[4].

For the advanced Radar ESM application one would like to realize the very fine frequency/phase discrimination of coherent techniques while maintaining accuracy over a wide bandwidth of interest.

This report describes the results of an investigation of a digital approach to quadrature demodulation to achieve superior stability and accuracy over a wide bandwidth and for short pulses. Error boundaries, performance evaluation, and means of reducing complexity for possible application specific integrated circuit implementation were also studied.

2.0 DIGITAL QUADRATURE DEMODULATION FOR RESM

2.1 DIGITAL VERSUS ANALOG QUADRATURE DEMODULATION

Coherent quadrature demodulation[1] has application for within-pulse feature extraction because of its potential to facilitate the measurement and exploitation of very small phase or frequency changes over short time periods.

The standard analog implementation is shown in Fig. 1. Two mixers are used to mix the incoming IF signal with the reference signal and a 90° phase-shifted version of the reference signals. Low pass filters are then used to eliminate the unwanted sidebands. The resulting signals are called the in-phase and quadrature channels respectively. Usually the mixers mix the incoming IF signal spectrum to a position nominally centred around DC. In this case the resulting pair of signals are collectively called the *baseband quadrature signal.*

In the figure we have assumed that subsequent processing will be digital, and therefore two analog-to-digital converters follow the low-pass filters. Mixing down to baseband minimizes the sampling rate required by the analog-to-digital converters. This directly yields the most economical representation of a given signal, reducing subsequent processing demands.

Note that two mixers are used to mix the same incoming signal with trivially different reference signals. The fact that there are two mixers leads to practical problems in matching the in-phase and quadrature channels in terms of their gain and phase. If the reference is not exactly 90° out of phase, the I/Q representation is not truly orthogonal. A gain imbalance will also distort the signal by scaling the complex axes, leading again to phase and amplitude errors which will compromise subsequent processing.

The typical overall phase accuracy for a good analog system has been reported at $1° - 2°$. Phase and amplitude correction can improve this performance, but incurs a significant increase in system cost and complexity[5, 6].

A digital implementation is shown in Fig. 2. Note that there is no mixing to baseband and that there is only one analog-to-digital converter rather than two. The converter must work at a faster sampling rate than is the case in Fig. 1. This implies that the A/D converter must have good performance over the signal bandwidth centred about a suitable intermediate frequency. Consequently, parameters affecting high frequency performance such as aperture uncertainty time are important. Modern flash A/D converters show significant progress in this respect. For example an 8-bit A/D converter having a

[1]In this report the terms coherent quadrature demodulation, I/Q demodulation, in-phase and quadrature demodulation, and coherent detection are used interchangeably.

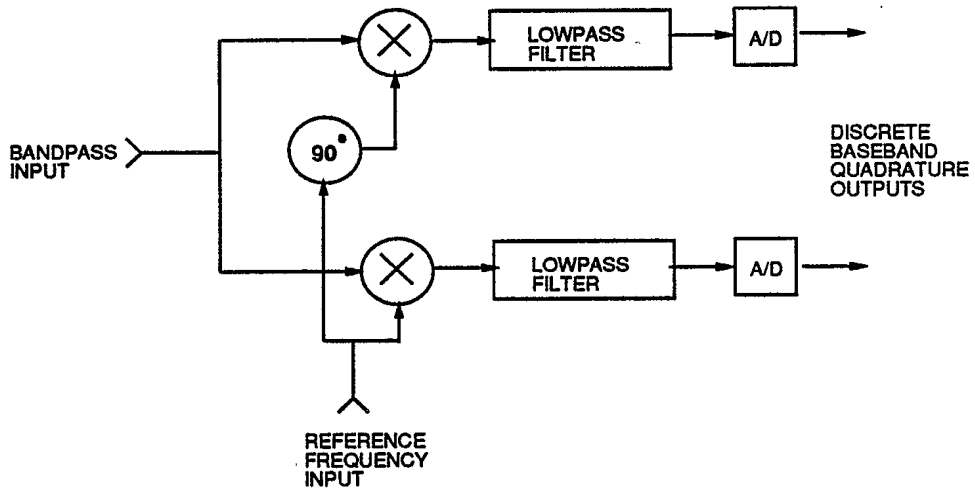

Figure 1: Standard analog implementation of an I/Q demodulator.

sampling rate of 650 MHz at which 7.8 bit effective resolution is achieved for a 150 MHz sinewave has been reported[7].

The digital processor accepts the digital input data stream and produces a pair of digital output data streams which constitute the quadrature pair. Note that there is no reason that the digital demodulator cannot translate the signal down to baseband and output the baseband quadrature signal representation at the same low rate achievable in the analog system. However, the demodulator itself must be able to process the high-speed stream of digital data from the analog-to-digital converter.

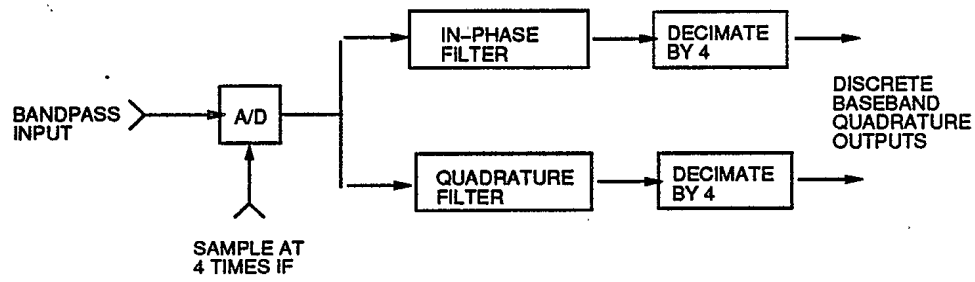

Figure 2: Digital implementation of an I/Q demodulator.

The digital implementation offers the ability to make tradeoffs between performance and computational cost. Additional benefits are that the system requires little in the way of tuning and maintenance and can be easily reproduced without careful attention to gain and phase matching of analog components. Furthermore, the analog signals need not be mixed down to baseband, with the result that some $1/f$ noise and possible DC

offset problems in the mixer are avoided. It does require a high-speed digital processor, but through the use of architectural techniques such as pipelining and parallelism, a compact and potentially cost-effective digital processor may be realizable as an application specific integrated circuit (ASIC). This is particularly true if care is taken to simplify the design of the digital filters by the appropriate choice of sampling and IF frequencies, and appropriate specification of the filter characteristics.

2.2 THE DIGITAL DEMODULATION TASK

The real bandlimited IF signal from an RESM receiver can be written as follows :

$$\begin{aligned} r(t) &= A(t)\ \cos[\omega_o t + \phi(t)], && (1)\\ &= A(t)\ \cos\phi(t)\cos\omega_o t - A(t)\sin\phi(t)\sin\omega_o t, && (2)\\ &= I(t)\cos\omega_o t\ -\ Q(t)\sin\omega_o t. && (3) \end{aligned}$$

The baseband in-phase and quadrature signals are $I(t) = A(t)\cos\phi(t)$ and $Q(t) = A(t)\sin\phi(t)$, and ω_o is the carrier in radians per second. As long as the bandpass signal $r(t)$ is sampled at the Nyquist rate (greater than twice the highest frequency component), the information in the signal is preserved and, in principle, digital I/Q demodulation can be performed. In practice it is useful to observe what happens when the sampling frequency f_s is chosen such that $f_s = 4f_o$, where f_o is the IF centre[2] frequency, i.e., $f_o = \frac{\omega_o}{2\pi}$. As reported by Waters and Jarret[8], the discrete sequence $r(t_n)$ will be:

$$\begin{aligned} r(t_n) &= (-1)^{n/2} I(t_n) \qquad n \text{ even} && (4)\\ &= (-1)^{(n-1)/2} Q(t_n) \qquad n \text{ odd.} && (5) \end{aligned}$$

This was obtained by simply substituting $t = t_n = n\frac{1}{4}f_o = n\frac{\pi}{4}$ into 3. In [8] it is observed that the true I and Q signals can be obtained by splitting the even and odd samples into separate sequences and then multiplying these sequences by an alternating sequence of plus and minus ones. The only remaining difficulty is that interpolation is required to obtain I/Q pairs at the same instant in time. A particular type of interpolator is suggested in [8] and good results claimed in limited tests. A problem with this approach is that an interpolator is most easily understood in the time domain, and in the analysis given no attention is paid to the frequency domain behaviour. This means there is no rational basis by which one can predict and design for good wideband performance, which is to say that it is difficult to say how the demodulator will perform on any but the particular test signals used. This issue is of concern given the wide bandwidths needed in the radar ESM application.

Thiel and Saulnier[9] used a similar analysis and a simple two-point average

[2]Note that the term *centre frequency* refers to the centre of the available receive bandwidth. The incoming baseband signal will generally be centred at some other frequency within the wide bandwidth of the ESM receiver.

interpolator, but have also introduced a simple filter to remove DC offsets. This addresses an important practical issue, and is potentially useful for narrow band radio signals. Again, however, the interpolation analysis does not allow us to evaluate the design's performance over a wide bandwidth. As will be shown in section 2.4.1, the Thiel and Saulnier design is of little use in the RESM context.

We can gain insight into the sampled signal through a graphical interpretation. Figs. 3A and 3B show an IF signal bandlimited to f_o before and after sampling at 4 times f_o.[3] What we would like to obtain is one of the sidebands of Fig. 3B translated to zero frequency as shown in Fig. 3C. Note that since the single sideband is generally asymmetric, the signal must be complex. Since one sideband is simply the antisymmetric image of the other sideband, we can get rid of one redundant sideband and sample at f_o without losing information, thereby reducing downstream processing and storage demands.

One way to translate one of the sampled sidebands to baseband is to multiply the sampled IF signal by a complex exponential at frequency f_o. This is shown in Fig. 3D. The complex exponential samples will take the values $[1, j, -1, -j, 1, j, -1, -j, ...]$. Thus it can be seen that splitting the sequence into even and odd samples and multiplying by plus and minus ones is equivalent to a frequency translation. Therefore the interpolation step is equivalent to a complex filter which removes the extraneous sideband at $2f_o$. Unfortunately, the early treatments do not use this physical interpretation, and therefore do not benefit from a filter-design approach. More recent papers by Rempel and Haslam[10], and April[11] do take a filter design approach however.

A natural step should be to decimate the complex signal shown in Fig. 3C by a factor of four, since all the information will be preserved if the bandwidth of the signal is less than or equal to f_o. This bandwidth constraint is unlikely to be critical in practice since it is difficult to design analog IF filters having larger relative bandwidths. The signal after decimation is illustrated in Fig. 3E. Given that this is done, we can note that only every fourth sample of the in-phase channel is needed, and we can avoid multiplying the in-phase channel by plus and minus ones.

Another approach to demodulation is to eliminate one sideband, and then achieve the frequency translation by simply decimating by four. The decimation by four aliases the complex modulation signal down to baseband. This approach is taken by Mitchell[12].

[3]It is also interesting to note what happens when a narrow baseband signal is sampled at $\frac{4}{3}f_o$, or $\frac{4}{2M-1}f_o$ where M is an integer. These rates were suggested in [8]. It turns out that that the signal band gets aliased down such that the actual sampling rate remains four times higher than the 'new' aliased IF. Therefore the discussion in this report can be generalized to these other sampling rates as long as the signal bandwidth is narrow enough to fit within the available bandwidth after decimation to baseband.

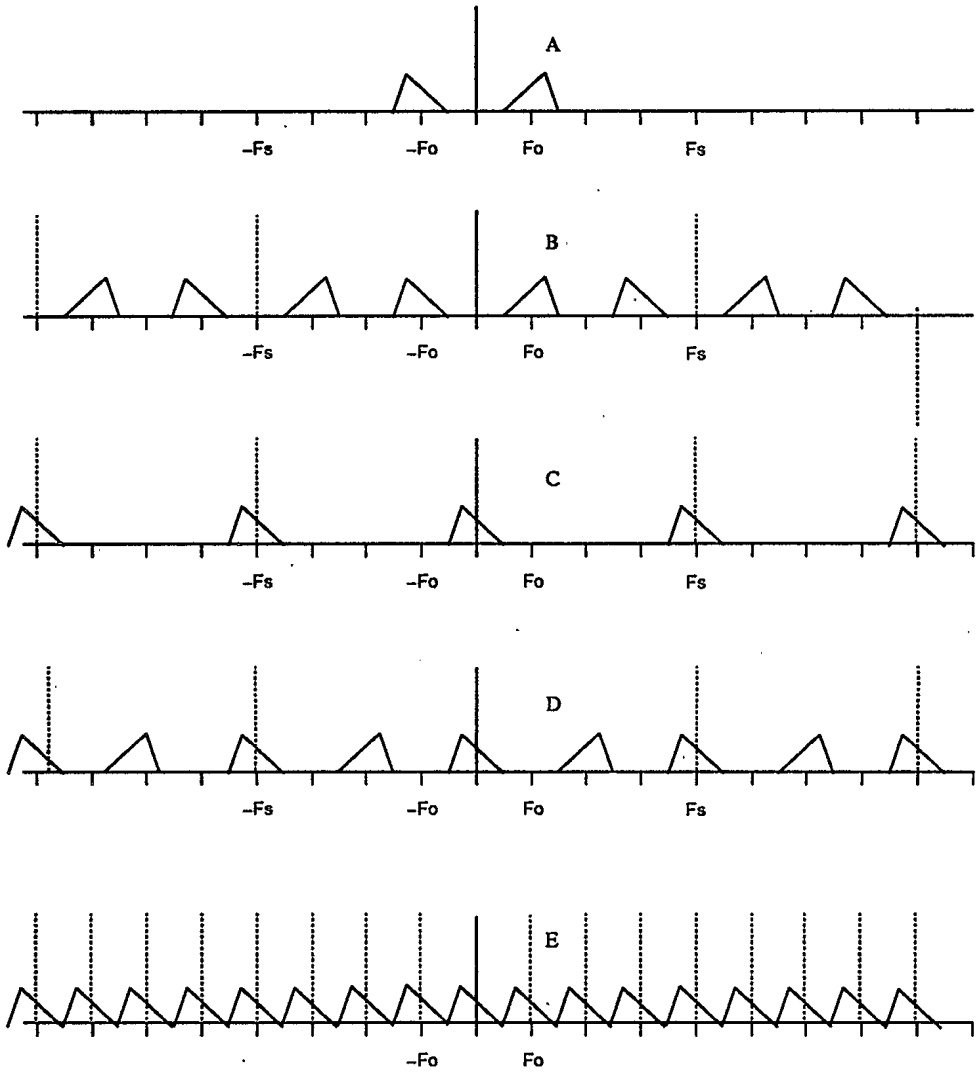

Figure 3: Signal spectra at various demodulation stages.

Inspection of the filter coefficients which arise from these approaches reveals that the multiplication by plus and minus ones as in [8] appears as alternating coefficient signs in the sideband removal filters. These two approaches are conceptually different, but are computationally similar. Like Waters and Jarret, Mitchell filters only the Q channel. Mitchell's approach has the virtue of being designed to known frequency response specifications.

The papers by Roy and Inkol[13] and Lodge[14], like Thiel and Saulnier, also make an attempt to remove the DC offsets introduced by the A/D converter by the use of filters in both the I and Q channels. In [13] it is suggested that bandpass filters with identical amplitude reponses but a 90° phase offset be used.

The following section presents three separate design approaches for the digital demodulator filter bank, each with varying degrees of complexity and performance. An extremely simple design can be used if moderate[4] bandwidths on the order of 60% of f_o are sufficient and if the DC offsets (in one channel only) at the output of the digital demodulator can be controlled or compensated for outside of the demodulator. A more complex design eliminates DC offsets at moderate bandwidths. A third design approach can provide, at about the same level of complexity, excellent phase fidelity over a wide bandwidth (approaching 100% of f_o) with no DC offset problems, but with relatively more shaping of the amplitude response. One very effective example of this last approach requires only nine unique coefficients for the pair of filter banks and 17 real multiplies per complex baseband output sample.

[4]Moderate is a relative term. A bandwidth of 60% would likely be considered wideband by communications standards. For the RESM application, however, very wide bandwidth is required, especially for digital demodulation where increases in the IF frequency may be constrained by practical sampling rates.

2.3 THREE DEMODULATOR DESIGN APPROACHES

2.3.1 Medium BW Design With Simple Hilbert Transformer

In this design, the quadrature channel only is filtered as shown in Fig. 4. The goal of the filtering is to provide a very flat frequency response centred around $\frac{f_s}{4} = f_o$ and 90° phase for a bandwidth on the order of 40-60% of f_o. A filter which meets this requirement is the Hilbert transformer.

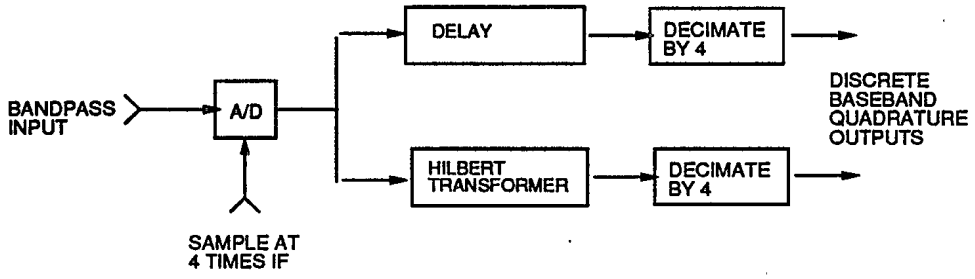

Figure 4: The Medium Bandwidth Simple Hilbert Transformer Design.

The ideal Hilbert transformer is a 90° phase shifter at all frequencies, and has an infinite impulse response. A finite impulse response approximation to the Hilbert transformer can be designed to any desired order.

For obtaining the flat equiripple response that is desirable for our application, the Parks-McClellan algorithm may be used[15]. Fig. 5 shows the magnitude of the frequency response for sixth order (7 tap) FIR Hilbert transformers for transition bandwidths of $0.2f_s$, $0.15f_s$ and $0.1f_s$. These correspond to passbands of 40%, 80% and 120% of f_o, the IF frequency. Although ripple is very noticeable for the wider passbands, the ripple amplitude is on the order of -50 dB for the transition bandwidth of $0.2f_s$.

The coefficients of the filters of Fig. 5 are given in Table 1. Note that the coefficients are anti-symmetric, and that every other coefficient is zero. The anti-symmetry is a consequence of the 90° phase condition, and the zero coefficients appear because of the symmetry of the frequency response about $\frac{f_s}{4}$.[5]

With this design and using the sixth order filter, only two unique coefficients are required. The Q component can be implemented in this case using only 3 real adds and two real multiplications:

[5]This symmetry would disappear if unequal ripple in the pass and stop bands were specified. Therefore it is undesirable to use the ripple weighting parameter of the Parks-McClellan algorithm to try to optimize flatness in the passband.

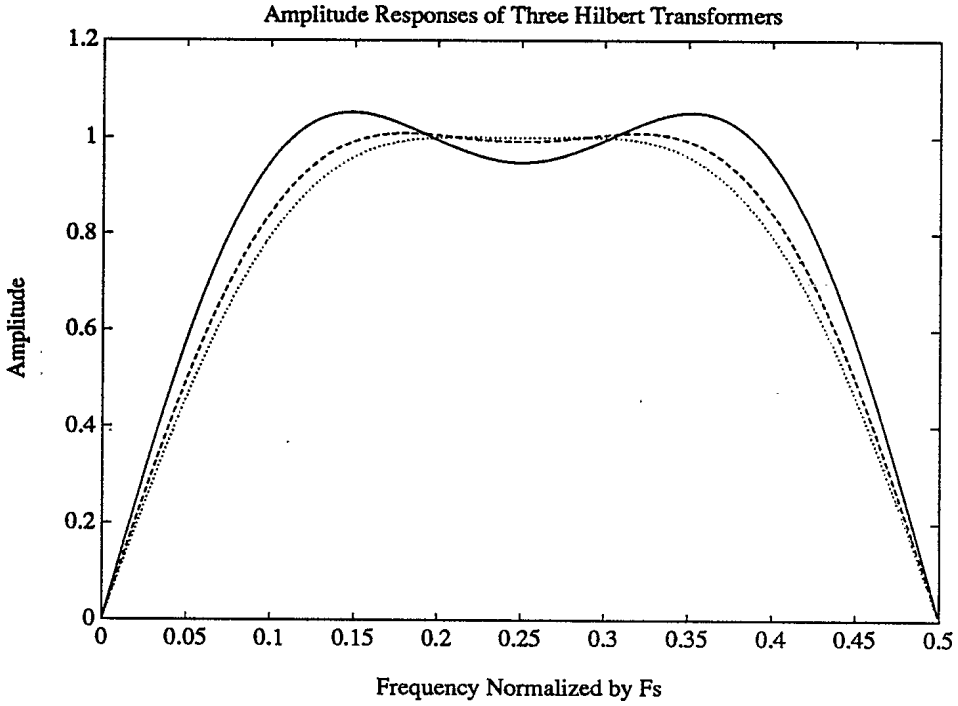

Figure 5: Amplitude Responses of 6th order Hilbert transformers with transition bandwidths of 20% f_s (dotted line), 15% f_s (dashed line) and 10% f_s (solid line), corresponding to passbands of 40%, 80% and 120% of f_o.

Table 1: Sixth order Hilbert transformer coefficients..

Bandwidth							
40% f_o	-0.0674	0.0000	-0.5672	0.0000	0.5672	0.0000	0.0674
80% f_o	-0.0848	0.0000	-0.5805	0.0000	0.5805	0.0000	0.0848
120% f_o	-0.1272	0.0000	-0.6013	0.0000	0.6013	0.0000	0.1272

$$y(n) = k_1[r(n-1) - r(n+1)] + k_2[r(n-3) - r(n+3)] \quad (6)$$

Since the final result is decimated by 4 to baseband, the computation above need only be evaluated at the rate of $\frac{f_s}{4}$. As mentioned above, the I component is obtained merely by delaying the signal (to match the 3 sample delay of the Hilbert transformer) and decimating by a factor of four. The odd number of taps ensures that the Q component is available co-incident in time with the I component.

2.3.2 Medium BW Design With Zero DC Offset

In this design approach we modify the simple design of the previous section by introducing a filter into the in-phase channel for the purposes of removing DC offsets which may be introduced by the analog-to-digital converter.[6] This is shown schematically in Fig. 6.

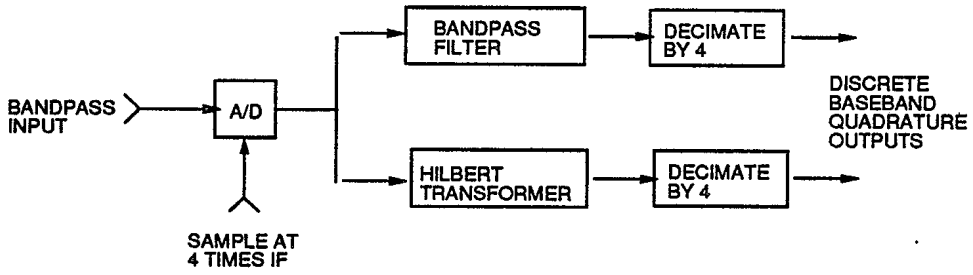

Figure 6: The Medium Bandwidth Design with DC Offset Removal.

The DC offset is introduced by the analog-to-digital converter and lies at true DC as observed at the intermediate frequency, not the DC after the modulator has translated the complex modulation signal to baseband.

In order to keep the filters as simple as possible, only halfband filters were considered. To achieve further simplification, the filters proposed by Goodman and Carey [16] were used. Since these use binary coefficients having few non-zero digits, multiplications can be economically implemented in binary arithmetic by shift and add operations.

The design procedure is to take the halfband low pass filters of [16], which already had nearly every other coefficient zero, and intersperse zeros between each coefficient. This is equivalent to a compression of the frequency scale (expansion of the time scale). Next, the filter is translated to $f_s/4$ by multiplying by a cosine at that frequency. This procedure

[6] It should be noted that the Hilbert transformer filters in the quadrature channel always have a null at DC, and therefore have no DC offset problem.

also has the advantage that no new non-zero coefficients beyond those used for the original filters were required.

Fig. 7 and Fig. 8 show the before and after results of this operation on the frequency response of the filter for the so-called F5, F6 and F7 filters.[7] In Fig. 7 the solid line is for the F5 filter, the dotted line is for the F6 filter and the dashed line is for the F7 filter. All of the original filters are eleven-tap filters with 7 non-zero coefficients. Due to the symmetry of the impulse reponse, only 4 of the non-zero coefficients are unique. After conversion to a band-pass filter by interspersing zeros, the filters are 21-taps in length, but still have only 4 unique non-zero coefficients. Table 2 gives the coefficients for the F5, F6, and F7 filters as presented by Goodman *et al.*

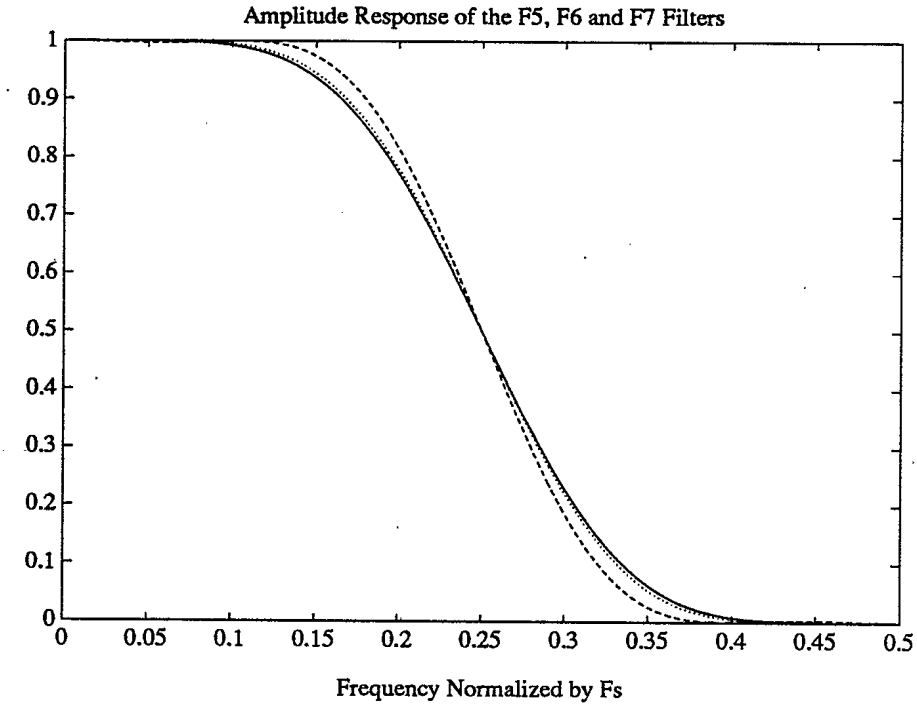

Figure 7: Amplitude responses of the Goodman-Carey F5, F6 and F7 filters, plotted as the solid, dotted and dashed curves respectively.

One small detail that should not be overlooked is that these filters have non-unity gain. Since the I and Q channels must be gain-matched, a final normalization is required after the filter to restore unity gain. The normalization factors are 512, 792 and 1024 respectively.

[7]The frequency responses have been normalized to 1 to facilitate comparisons.

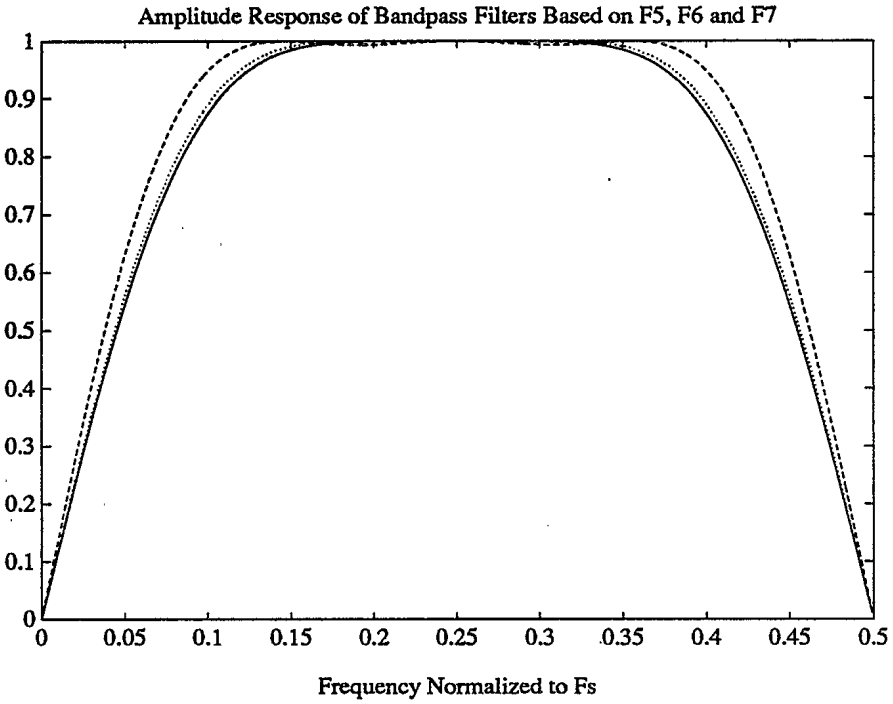

Figure 8: Amplitude responses of three bandpass filters based on the Goodman-Carey F5, F6 and F7 filters, plotted as the solid, dotted and dashed curves respectively.

Table 2: Coefficients for three of the Goodman-Carey filters..

Filter Name											
F5	3	0	-25	0	150	256	150	0	-25	0	3
F6	9	0	-44	0	208	346	208	0	-44	0	9
F7	7	0	-53	0	302	512	302	0	-53	0	7

2.3.3 Wide BW Matched Response Design With Zero DC Offset

A different design approach is taken in this design. With FIR filters, the sole source of phase error is amplitude imbalance between the FIR frequency responses of the two channels. Therefore we attempt to optimize the *similarity* of the frequency responses of the two channels rather than their flatness, while maintaining 90° relative phase. This approach is shown schematically in Fig. 9.

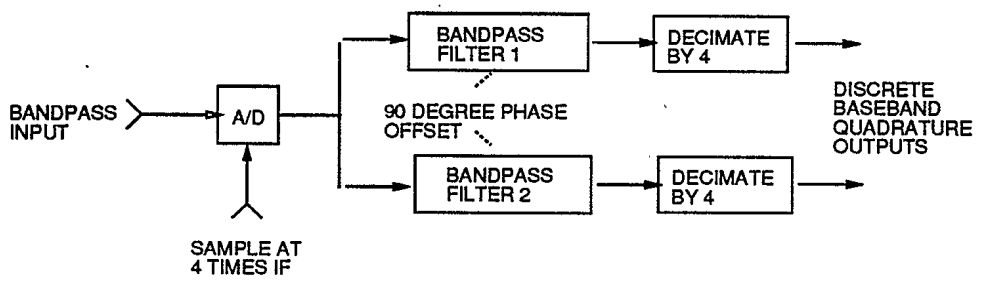

Figure 9: The Wide Bandwidth Design with Matched Response and DC Offset Removal.

The design procedure for the matched response filter is as follows:

1. Design an FIR low-pass filter with an odd number of taps.
2. Produce the in-phase channel bandpass filter by multiplying by $\cos(n\frac{\pi}{2})$.
3. Produce the quadrature channel bandpass filter by multiplying by $\sin(n\frac{\pi}{2})$.
4. Test the design as described in section 2.5, and iterate.

Steps two and three amount to a translation of the filter frequency response upwards by $\frac{1}{4}f_s = f_o$, where f_s is the sampling frequency and f_o is the IF frequency of the demodulator.

In this study the filter in step 1 was designed for a passband from DC to $\frac{1}{8}$ of the sampling frequency, using a Hamming window design procedure for various orders.[8] After steps 2 and 3 above, the frequency responses are half-band in form. The resulting filter coefficients have the following properties:

- The in-phase coefficients were symmetric and, except for an additional non-zero coefficient at the centre tap, only every fourth coefficient was non-zero.

[8]There is no reason other filter design procedures could not be used. Satisfactory results were obtained, so no attempt was made to try using other filter design procedures.

- The quadrature coefficients were anti-symmetric, with every other sample a zero.
- A given tap is never simultaneously non-zero for both the in-phase and quadrature channels.

The first two properties reduce the number of multiplications required for a given filter order. The third property indicates that the sample data can be demultiplexed into two separate and parallel processing chains. Typical filter coefficients, derived from the 21 tap FIR lowpass filter tested in section 2.5.4 are shown below. The coefficients b_i and b_q correspond to the in-phase and quadrature filters respectively.

$$b_i = \begin{bmatrix} -0.0048 \\ 0.0 \\ 0.0 \\ 0.0 \\ 0.0413 \\ 0.0 \\ 0.0 \\ 0.0 \\ -0.2896 \\ 0.0 \\ 0.5 \\ 0.0 \\ -0.2896 \\ 0.0 \\ 0.0 \\ 0.0 \\ 0.0413 \\ 0.0 \\ 0.0 \\ 0.0 \\ -0.0048 \end{bmatrix} \quad b_q = \begin{bmatrix} 0.0 \\ 0.0049 \\ 0.0 \\ 0.0168 \\ 0.0 \\ -0.0479 \\ 0.0 \\ -0.1209 \\ 0.0 \\ 0.4397 \\ 0.0 \\ -0.4397 \\ 0.0 \\ 0.1209 \\ 0.0 \\ 0.0479 \\ 0.0 \\ -0.0168 \\ 0.0 \\ -0.0049 \\ 0.0 \end{bmatrix} \tag{7}$$

2.4 CHARACTERIZATION OF QUADRATURE DEMODULATORS

In the literature, quadrature demodulators are often designed for narrow band signals. As such, it is often difficult to predict the usefulness of a given design for applications requiring wide bandwidths.

A frequency domain characterization is useful in order to gain an understanding of performance over a wide bandwidth. This is important because the radar signals received by an RESM receiver may be translated by many Megahertz in frequency due to frequency agility of the radar, or due to initial uncertainty of the carrier frequency. Good performance over a wide bandwidth is also consistent with the requirement to process short pulse signals.

Time domain characterization is also important. While frequency domain characterizations can indicate performance over a bandwidth, it is also useful to have time domain results. These allow one to determine *where* errors occur during a pulse, and to characterize them in terms of error magnitudes. For instance in the RESM application the leading edge of the pulse is potentially very important because it is relatively free of multipath influences. Knowledge of the size and distribution of phase errors over time can be useful in judging the likely usefulness of the demodulator output for given applications. Also some nonlinear effects such as quantization effects are best evaluated in the time domain.

2.4.1 Slow Chirp Simulation

The slow chirp test consists of injecting a simulated unit-amplitude sinusoidal IF with a frequency that slowly varies at a constant rate into the demodulator model. The input signal thus exercises the demodulator over a wide range of frequencies, but changes slowly enough that transient effects are not observed.

The complex output of the demodulator is then compared with the analytically derived result, which is simply a unit amplitude complex exponential with the same linear frequency ramp, but translated in frequency so that the IF is mapped to DC. This method of analysis allows phase and amplitude errors to be measured directly.

For the chirp test we generated a standard real input signal of the following form:

$$r(t) = \cos[2\pi(f_i + \frac{f_m}{2}t)t)] \tag{8}$$

We used the values $f_i = 10$ MHz, $f_m = 0.6$ MHz/usec. The signal was evaluated over the interval $0 \leq t \leq 50$ usecs. In the tests shown, a sampling rate of 100 MHz

was used, though the results are normalized to the sampling frequency and are generally applicable.

The ideal output of the demodulator will be

$$z(t) = (e^{j2\pi(f_i - f_o + \frac{f_m}{2}t)t})^* \tag{9}$$

where f_o is the IF frequency and * is the conjugate operator, necessary because of the definition of the quadrature component as derived in section 2.2.

Fig. 10 and Fig. 11 show the results of the slow chirp test when applied to Thiel and Saulnier's simple demodulator with DC offset removal described in [9]. This demodulator corresponds to trivial FIR filters described by the coefficients b_i and b_q for the in-phase and quadrature channels respectively[9]:

$$b_i = \begin{bmatrix} -0.25 \\ 0 \\ 0.5 \\ 0 \\ -0.25 \end{bmatrix} \quad b_q = \begin{bmatrix} 0 \\ 0.5 \\ 0 \\ -0.5 \\ 0 \end{bmatrix} \tag{10}$$

Fig. 10 shows the amplitude of the complex demodulator output relative to the ideal analytic result over the chirp. The instantaneous frequency of the chirp is shown along the horizontal axis. The amplitude performance shows that the demodulator of Thiel and Saulnier is not particularly flat, varying by almost 10% over a bandwidth of approximately 10% of f_s, i.e. 40% of f_o. The slow chirp amplitude result also shows an oscillation within an envelope defined by the amplitude responses of the two filters. The oscillations occur as the baseband signal phase changes and the relative contributions of the in-phase and quadrature channels varies.

Fig. 11 shows that the phase errors are small only for very small bandwidths. Over only 10% of f_s, phase errors reach 2°.

2.4.2 Filter Frequency Response and Phase Error Bounds

The magnitudes of the filter frequency responses for the demodulator's quadrature filter pair can be used to derive the maximum phase (and amplitude) errors that could appear at the various frequencies. This is useful because, as we have observed in the previous

[9]We actually had to exchange the I and Q filters and negate the coefficients of the Q channel in order to maintain consistency with the definition in section 2.2. This was not necessary for the experimental analysis given in [9].

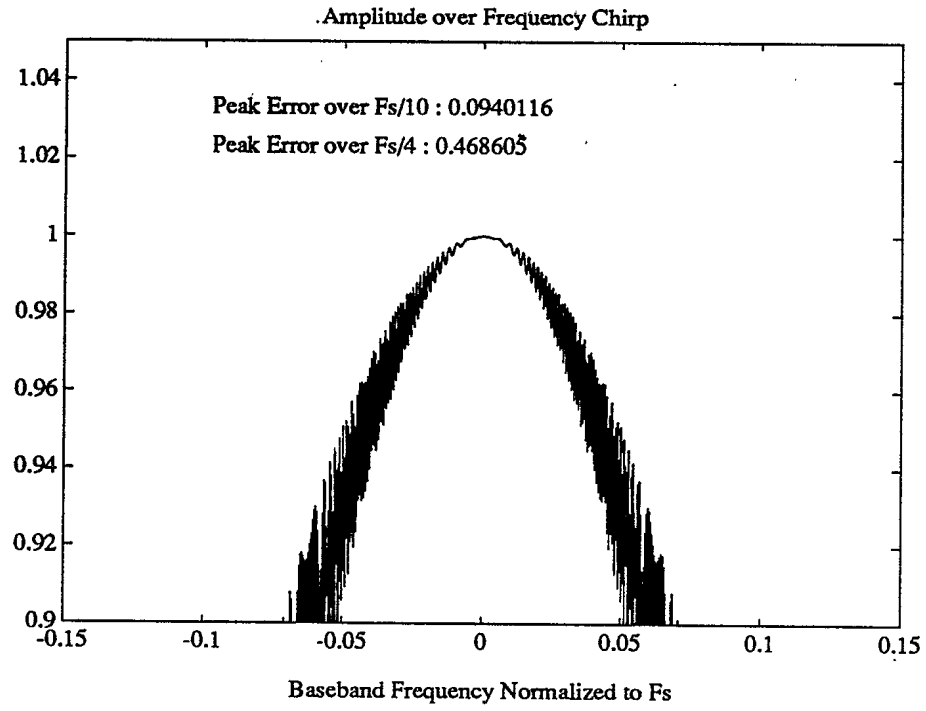

Figure 10: Amplitude performance of Thiel and Saulnier demodulator over a slow chirp.

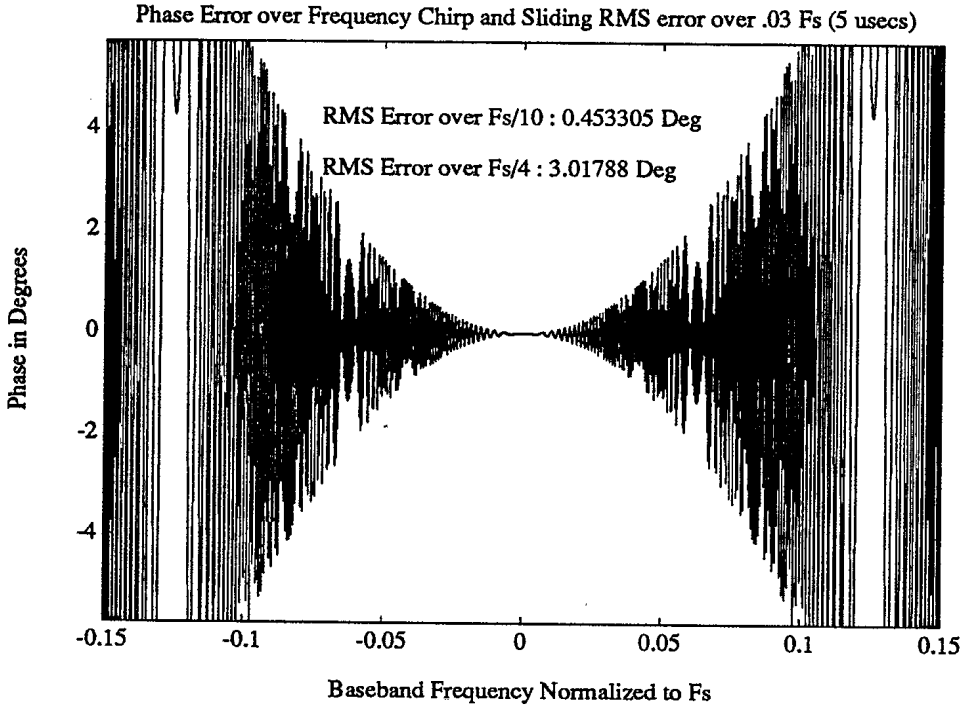

Figure 11: Phase performance of Thiel and Saulnier demodulator over a slow chirp.

section, the errors that can be measured in the time domain are dependent upon the baseband signal phase. A very small offset in frequency, time or initial phase can affect the results of the time domain test.

The FIR filters considered in this report have ideal phase characteristics. The only phase errors introduced by the filter pair are therefore those introduced by gain imbalances between the filters' amplitude response at any given frequency.

The maximum amplitude error comes from deviation of the filter amplitude responses from unity. The maximum amplitude error is due to the filter with the poorest amplitude performance at a given frequency, and is observed when the input signal has a phase of 0° or 180° when the in-phase channel is the limiting factor, and 90° or 270° when the quadrature channel is important. Amplitude errors are not dealt with in detail here, because the chirp test of Section 2.4.1 provides sufficient information for our needs.

A more serious problem is the phase error due to filter amplitude imbalance. Differences in the amplitude responses of the pair of filters cause a gain imbalance between the two channels. A sinusoidal input to the modulator should produce an output which traces out a circle in the complex plane at a frequency equal to the offset of the sinusoid frequency from f_o. When there is a gain imbalance, the complex signal traces out an ellipsoid instead of a circle, biasing the phase towards the axis (real or imaginary) with the greater gain.

The maximum phase error, ϵ_{max}, can be closely approximated given R, the ratio of the two channel gains:

$$\epsilon_{max} \approx \tan^{-1} R - \frac{\pi}{4} \tag{11}$$

The derivation of this equation may be found in appendix A.

To evaluate the phase error bound performance of demodulators we use the following procedure:

1. Compute the frequency responses of the in-phase and quadrature filters from their respective FIR coefficients.

2. Compute the ratio $R(\omega)$ by dividing the in-phase amplitude response by the quadrature amplitude response.

3. Compute and plot $\epsilon_{max}(\omega)$ using equation 11.

To show the usefulness of this approach, consider Fig. 12. This shows the phase error curve of Fig. 11 plotted along with the error bound curve. Note that the phase

error observed in the chirp test is bounded by the phase error maximum. In the chirp test the errors observed depend upon the particular phase at each sample. A decision made purely on the basis of a chirp test may underestimate the phase errors which might be experienced with other signals.

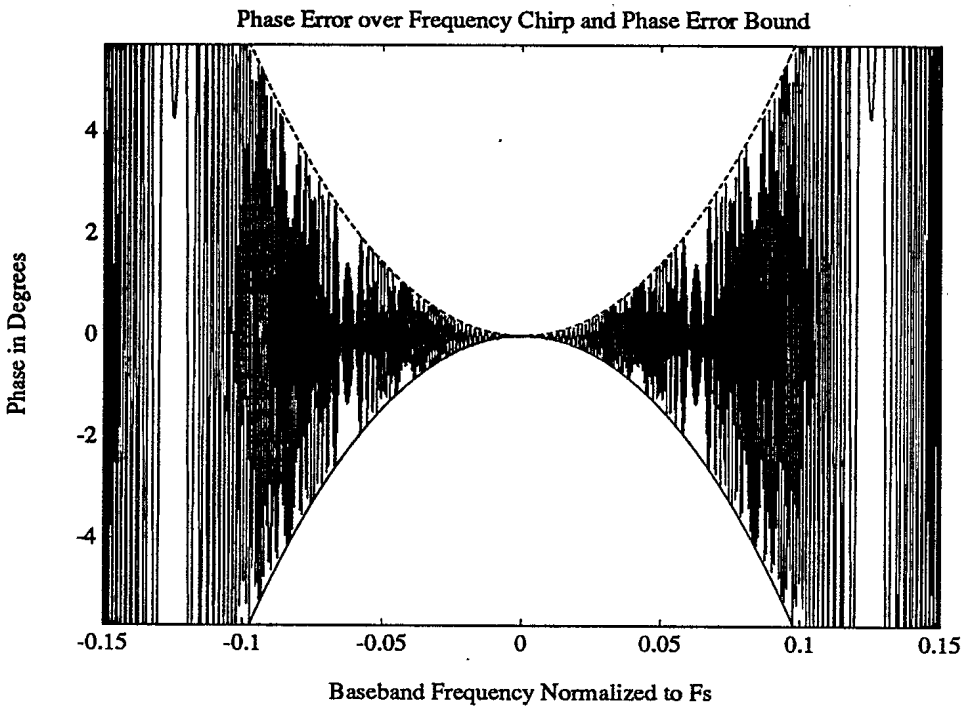

Figure 12: Phase performace of Thiel and Saulnier demodulator over a slow chirp, and the corresponding phase bound.

2.4.3 Pulse Signal Simulation

In the RESM application, a very fast transient response is required of the demodulator. Modulation information superimposed on potentially very short pulses must be reliably extracted. The leading edge of the pulse is of particular importance because it is relatively free of multipath effects.

For pulse signal simulations, we used the following procedure:

1. Generate real-valued pulses at IF of various widths and shapes (trapezoidal, raised cosine edges and Gaussian), modulated in a number of different ways.

2. Generate ideal complex baseband pulses which correspond to the real-valued pulses generated in step 1.

3. Demodulate the real pulses using the demodulator under study.

4. Compare the ideal baseband signals of step 2 with the outputs of step 3.

The results of the comparison are presented as plots of the ideal and experimentally derived signals over time, and in the form of plots of amplitude and phase errors over time.

2.5 EVALUATION OF DESIGNS FOR RADAR ESM

2.5.1 Phase Error Design Goals

In theory it is possible to design demodulation filters to meet any desired phase error performance at the expense of computational effort. In practice the phase error performance will be limited by factors other than the filters, such as A/D converter quantization error, jitter and non-linearity, and receiver noise figure.

A rational design for the demodulator filters then should provide sufficient precision so that the end-to-end phase error performance is not significantly influenced by the imperfections of the demodulation filters. Additional precision provides little benefit, and may in fact force sacrifices in other areas such as cost, power consumption and bandwidth.

Here we decided to base the phase error budget on the limits imposed on phase measurement accuracy by the number of bits resolved by the analog to digital converter. Table 3 shows the peak and RMS phase errors obtained when a full-scale amplitude vector with random phase is rounded to M-bit precision in I and in Q.[10] The results in this table are represented graphically in Fig. 13. For the limited purpose of estimating phase error design goals, these results were obtained by *Monte Carlo* experiment with 10,000 random phase vectors uniformly distributed over 2π.

Table 3: Peak and RMS phase errors due to quantization..

Bits	Peak Phase Error	RMS Phase Error
M = 6	1.26 deg	0.54 deg
M = 8	0.31 deg	0.13 deg
M = 10	0.078 deg	0.032 deg
M = 12	0.019 deg	0.008 deg

For the flash A/D converters required for a digital demodulator at RESM bandwidths, 8 effective bits of precision is likely to be the practical limit for the near future. Peak errors of approximately 0.3° are consistent with this precision.

[10]This does not correspond exactly to the situation for the digital demodulators considered. Some reduction in quantization noise might be expected because the demodulation filters will remove noise which falls in the stop bands of the filters. This is not expected to be a major effect since we are not oversampling by a large factor.

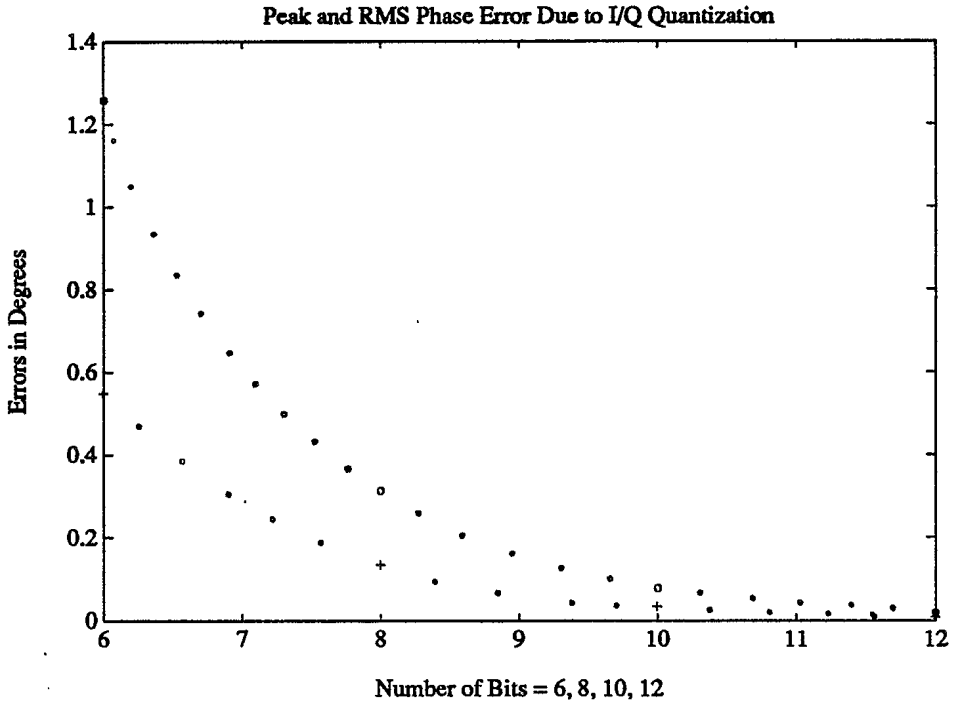

Figure 13: Peak and RMS phase errors due to quantization.

2.5.2 Medium BW Design with Simple Hilbert Transformer

In this section we present general findings and some key results for demodulator designs using simply a Hilbert transformer in the quadrature channel and a delay only in the in-phase channel.

In general we found that very low amplitude and phase errors could be achieved over a medium bandwidth with very modest filters. A seven-tap FIR Hilbert transformer with only two unique non-zero coefficients is sufficient to give nearly ideal results over a bandwidth equal to 40% of the IF. We used the Parks-McClellan filter design program to design Hilbert transformers with an odd number of taps. These always have zero coefficients for every other tap. Further, simplified coefficients having relatively few non-zero binary digits could be used at the cost of some loss in accuracy.

Fig. 14 shows the amplitude and frequency response for the Hilbert transformer defined by the coefficients

$$b_q = \begin{bmatrix} 0.0674 \\ 0 \\ 0.5672 \\ 0 \\ -0.5672 \\ 0 \\ -0.0674 \end{bmatrix} \tag{12}$$

This optimum 6th order Hilbert transformer is produced by the McClellan-Parks procedure for a transition bandwidth of 20% of f_s, the sampling frequency.

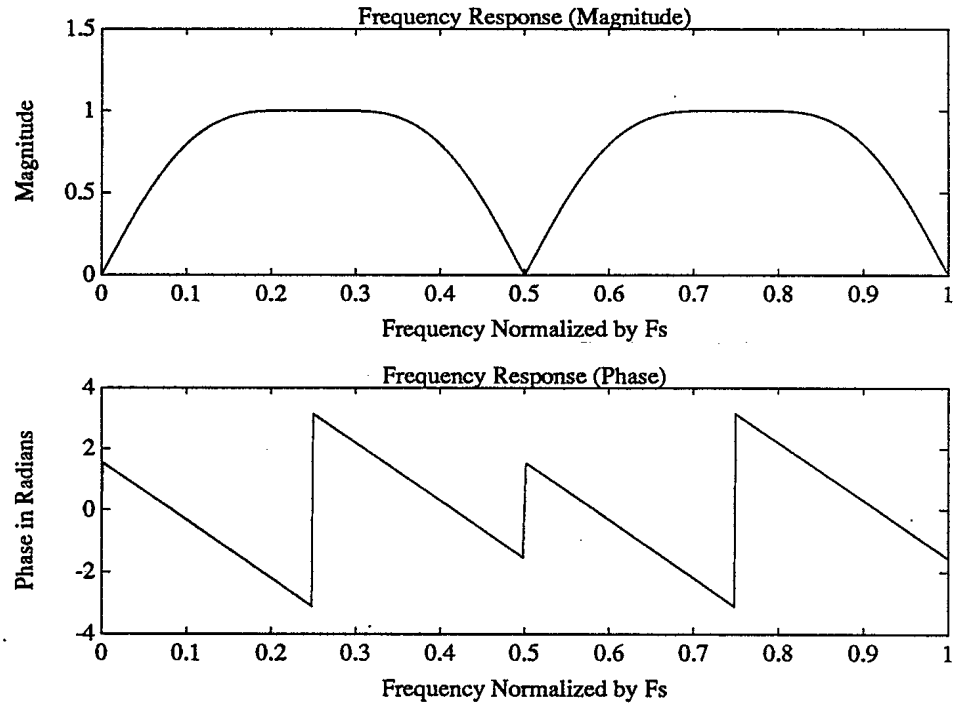

Figure 14: Amplitude and phase response of optimum 6th order Hilbert transformer, 20% transition band.

Fig. 15 and Fig. 16 show the results of the slow chirp test for this demodulator. Fig. 15 shows the amplitude of the complex demodulator output relative to the ideal analytic result over the chirp. The instantaneous frequency of the chirp is shown along the horizontal axis. The amplitude performance is extremely flat over about 10% of the sampling frequency, which corresponds to 40% of f_o, the IF. The phase performance is also a small fraction of a degree over this same range.

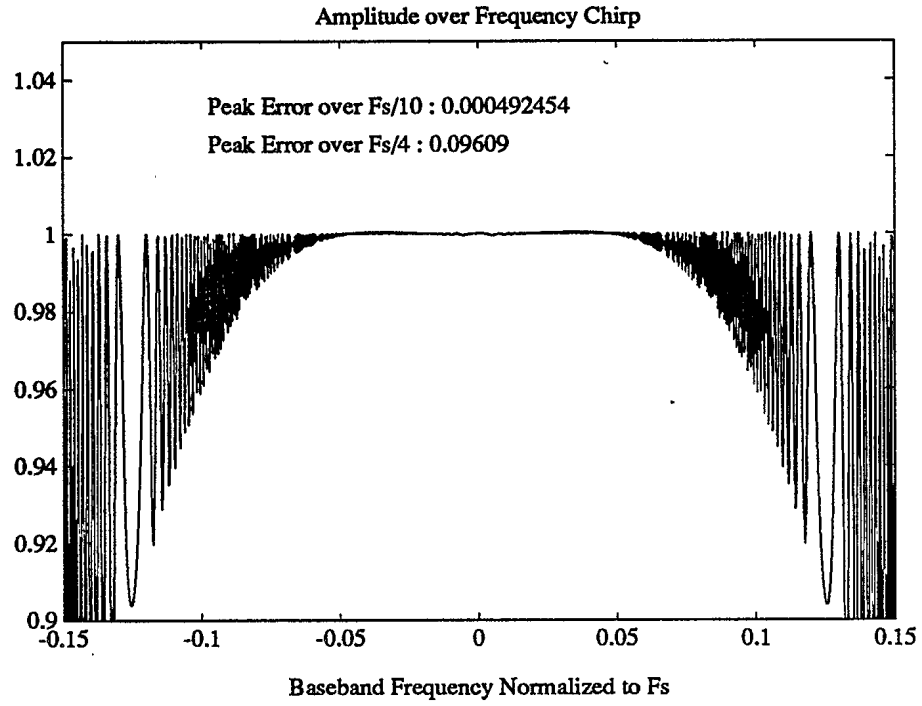

Figure 15: Amplitude performance of Optimum Hilbert demodulator over a slow chirp.

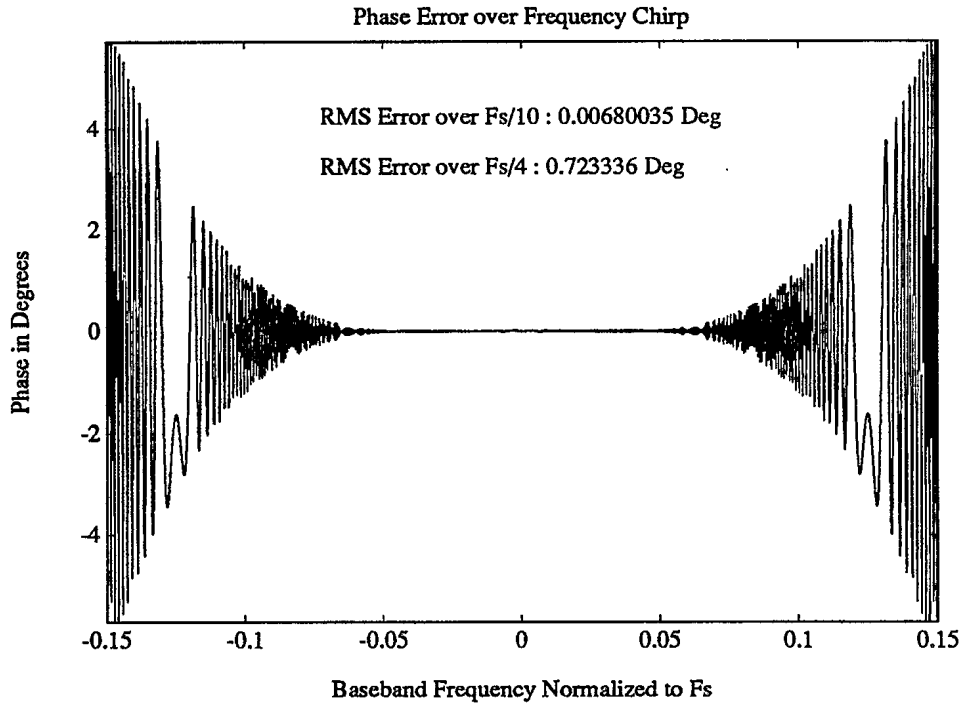

Figure 16: Phase performace of Optimum Hilbert demodulator over a slow chirp.

Performance degrades rapidly ouside of this range as the Hilbert transformer response rolls off.

The phase error bound is shown in Fig. 17.

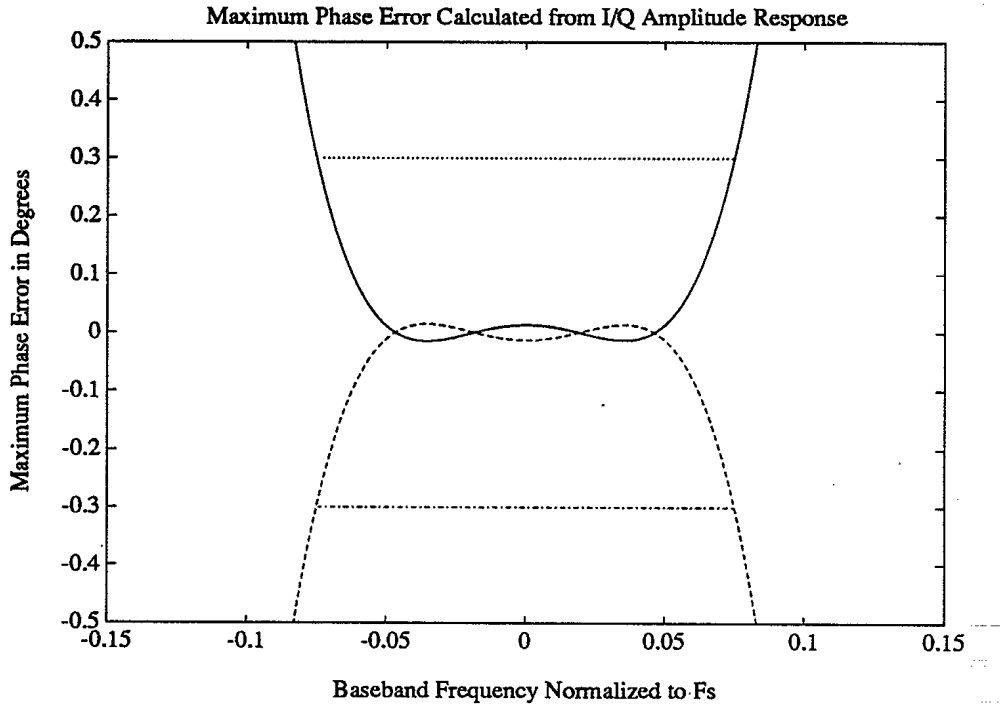

Figure 17: Phase error bound for the Optimum Hilbert demodulator, 40% f_o bandwidth. The horizontal lines indicate the 0.3° phase error design goal.

Other Hilbert transformer results were obtained, offering larger bandwidths at the expense of more serious phase errors. Up to 84% bandwidth can be obtained if phase errors of up to 0.3° can be tolerated (as per our phase error design goal), using only a sixth order filter. The phase error bound for this design is shown in Fig. 18. Further it was found that good Hilbert transformers could be obtained using simplified coefficients having few non-zero binary digits.[11]

A major flaw in this type of design is that it does not address the problem of DC offset in the in-phase channel. For this reason new approaches were investigated.

[11]One of these Hilbert transformers is given by equation 13 in the next section.

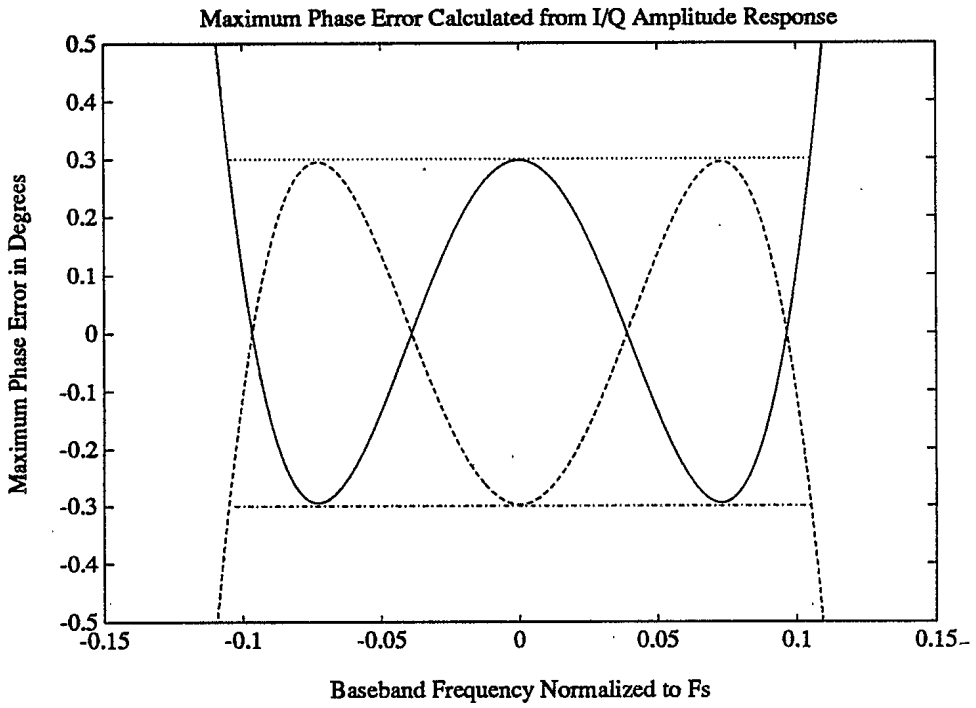

Figure 18: Phase error bound for the Optimum Hilbert demodulator, 84% f_o bandwidth. The horizontal lines indicate the 0.3° phase error design goal.

2.5.3 Medium BW Design with Zero DC Offset

For the medium bandwidth design with zero DC offset it was found that performances approaching those of the previous design could be achieved, but only with a significant increase in complexity. The elimination of DC offset involves introducing a bandpass filter into the in-phase channel. The problem is in designing a computationally economical bandpass filter to achieve the flat frequency response over a large relative bandwidth required to match the frequency response of the Hilbert transformer. As described in section 2.3.2, care was taken to ensure symmetry and a large number of zero taps. While the bandpass filter implementations are quite efficient, the bandpass filter required for the in-phase channel is of higher order than the Hilbert transformer.

The Hilbert transformer used in the quadrature channel is a variant of that in equation 11 of the previous section. In particular we used the filter defined by

$$b_q = \begin{bmatrix} 1 \\ 0 \\ 9 \\ 0 \\ -9 \\ 0 \\ -1 \end{bmatrix} \tag{13}$$

The frequency response of this filter[12] is shown in Fig. 19. This simplified transformer was also used during tests for the Medium Bandwidth Simple Hilbert transformer design and was found to be almost identical to the transformer of equation 11 except for a negligible decrease in the width of the flat portion of the frequency response.

The three Goodman and Carey filters mentioned in section 2.3.2 were tested as well as several others. The F7 filter gives the widest bandwidth with reasonable phase response. This can be predicted by examining Fig. 8, which shows the F7 filter to have a wide and flat response which matches well with the extremely flat response of Fig. 19.

The amplitude and phase slow chirp results are shown in Fig. 20 and Fig. 21 respectively. These results are comparable to those of the Medium Bandwidth design without the DC offset removal, though slightly degraded. This is to be expected given that the bandpass filter will not be perfectly flat. The phase error bound result is shown in Fig. 22.

Although there are only 4 unique coefficients required to implement the in-phase

[12]For convenience we have normalized the amplitude response to 1 in the passband.

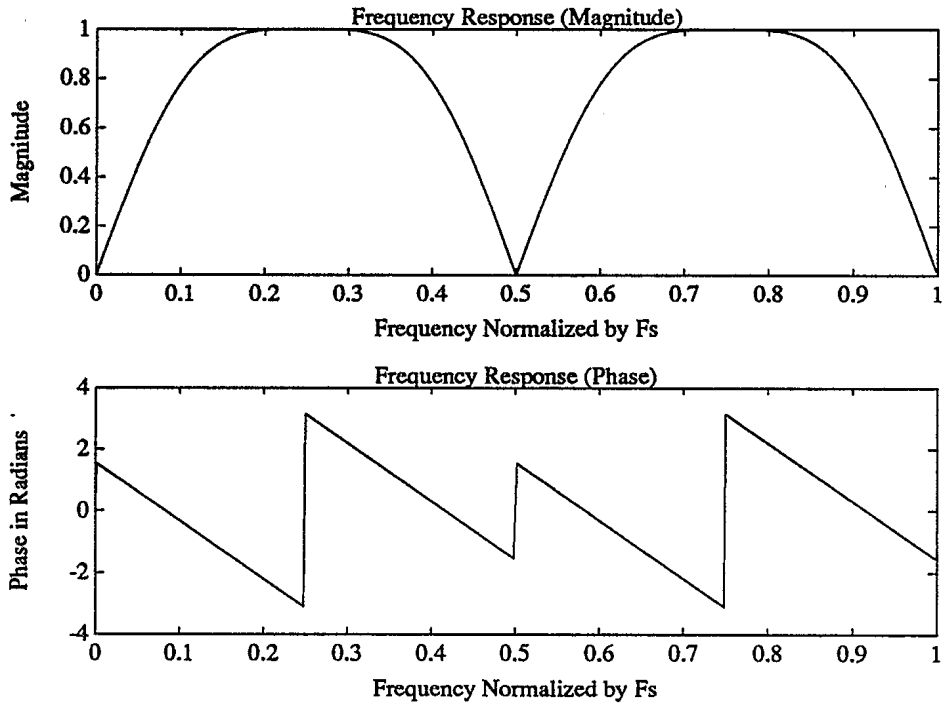

Figure 19: Frequency response for simplified Hilbert transformer.

filter, this is significantly more complex than the quadrature filter which has only two coefficients. The increase in complexity buys only a removal of the in-phase DC offset — the bandwidth is no better than the simple Hilbert design.

2.5.4 Wide BW Matched Response Design with Zero DC Offset

The wide bandwidth design based upon matched response filters was able to provide superior use of available bandwidth as well as zero DC offset. Three different demodulators of this type were tested using the chirp and phase error bound analyses described in sections 2.4.1 and 2.4.2. The most promising design was tested using a large set of pulse simulation runs, as described in section 2.4.3.

Hamming window designed filters with 13, 21 and 29 filter taps were studied.[13] The respective I and Q amplitude responses for each of these filter sizes are shown in Fig. 23, Fig. 24 and Fig. 25 respectively. The in-phase channel amplitude response is shown as the solid curve and the quadrature channel amplitude response is shown as the dotted curve.

[13]Filters with intermediate numbers of taps are no different from the filters studied, because the additional taps at the ends are all zeros.

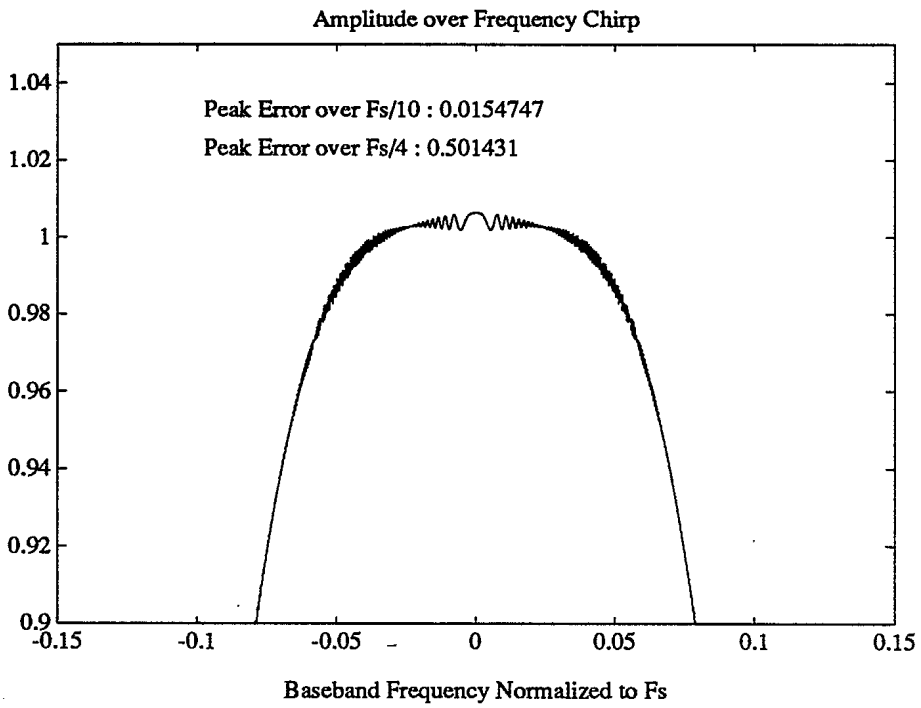

Figure 20: Amplitude performance of Medium-BW-Zero-DC demodulator over a slow chirp.

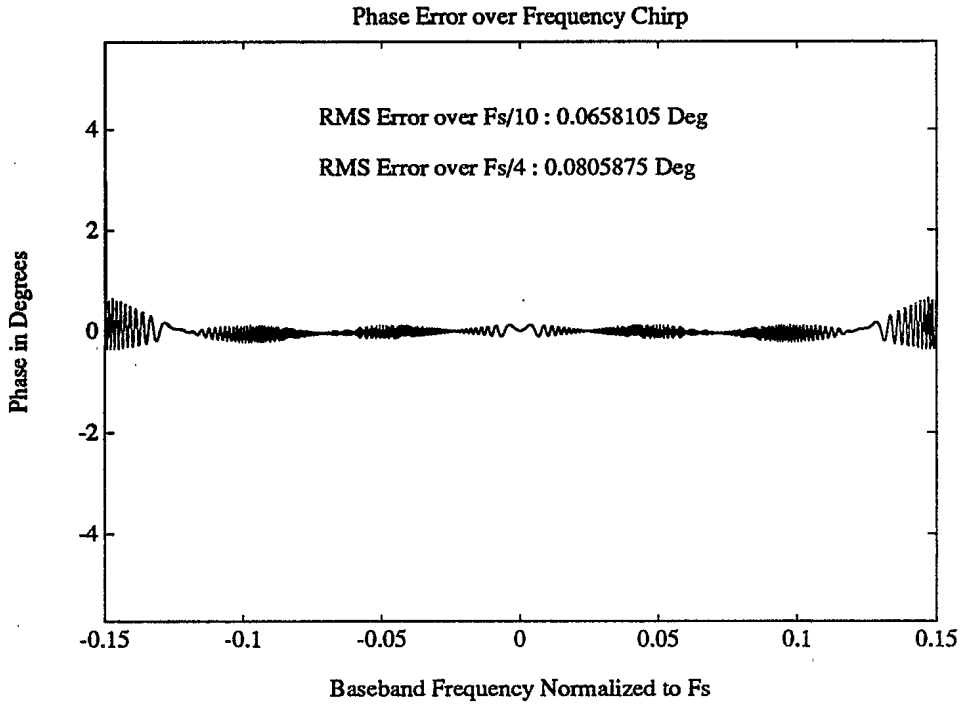

Figure 21: Phase performance of Medium-BW-Zero-DC demodulator over a slow chirp.

The longer filters provide better performance, both in terms of phase errors and amplitude flatness. The 21 tap filter pair was selected for further study because it provides a phase performance which exceeds the 0.3° design goal, and is less costly than the 29 tap filters which achieved about 0.1° peak error.

Fig. 26 and Fig. 27 show the chirp test results, and Fig. 28 shows the phase error bound result.

The 21 tap design was also tested with pulse signals. Additional results are presented to indicate the effects of the following modifications:

- The filter coefficients were rounded to nine bit precision.[14]
- The IF data was rounded to eight bit precision.

Performance was somewhat compromised by quantization, but was not seriously degraded. For this reason we show a series of results for the 21 tap matched response filter

[14]Care must be taken that the coefficients from both filters are scaled the same way to maintain channel gain balance. The quantization was set so that the largest magnitude coefficient in the filter pair was scaled to be simply as a nine bit shift operation and all other coefficients were scaled appropriately.

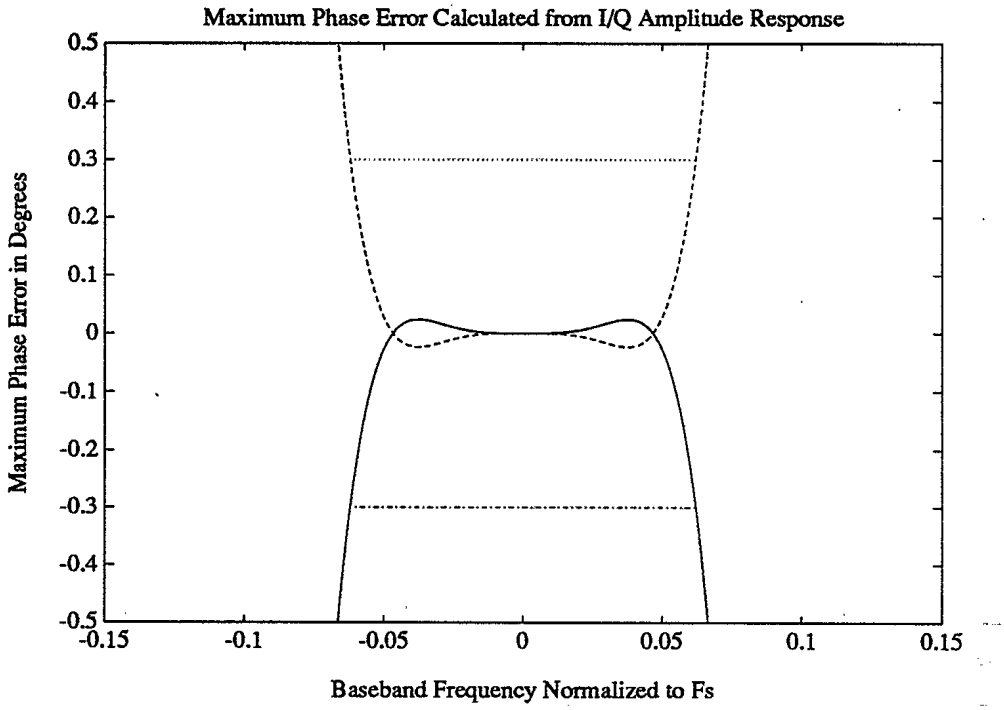

Figure 22: Phase error bound for the F7 Medium-BW-Zero-DC demodulator. The horizontal lines indicate the 0.3° phase error design goal.

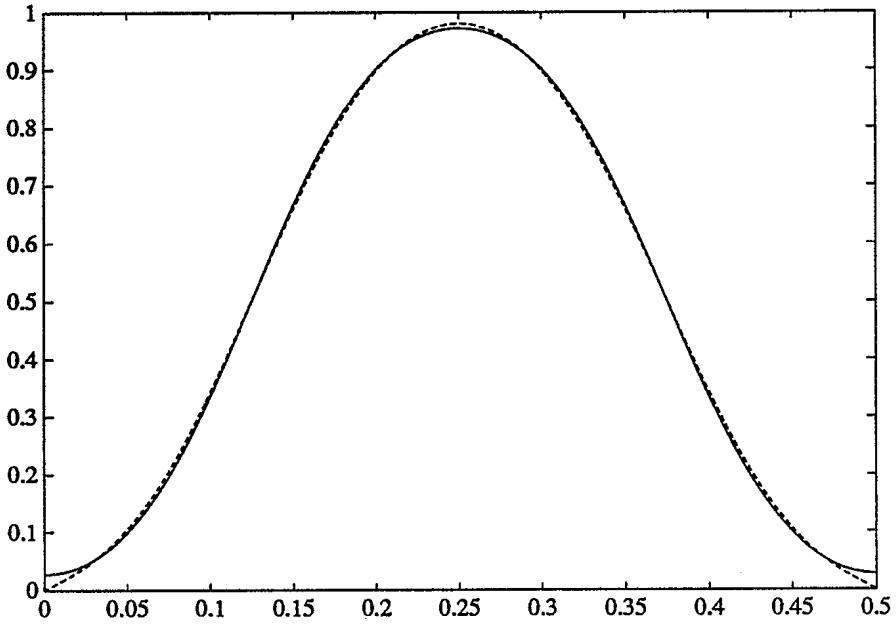

Figure 23: Matched amplitude responses for 13 tap filters.

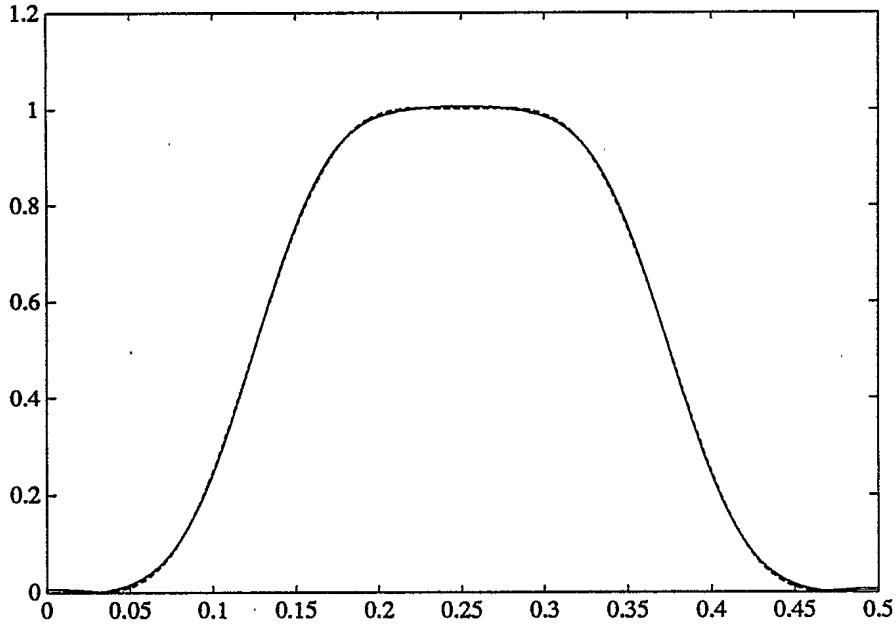

Figure 24: Matched amplitude responses for 21 tap filters.

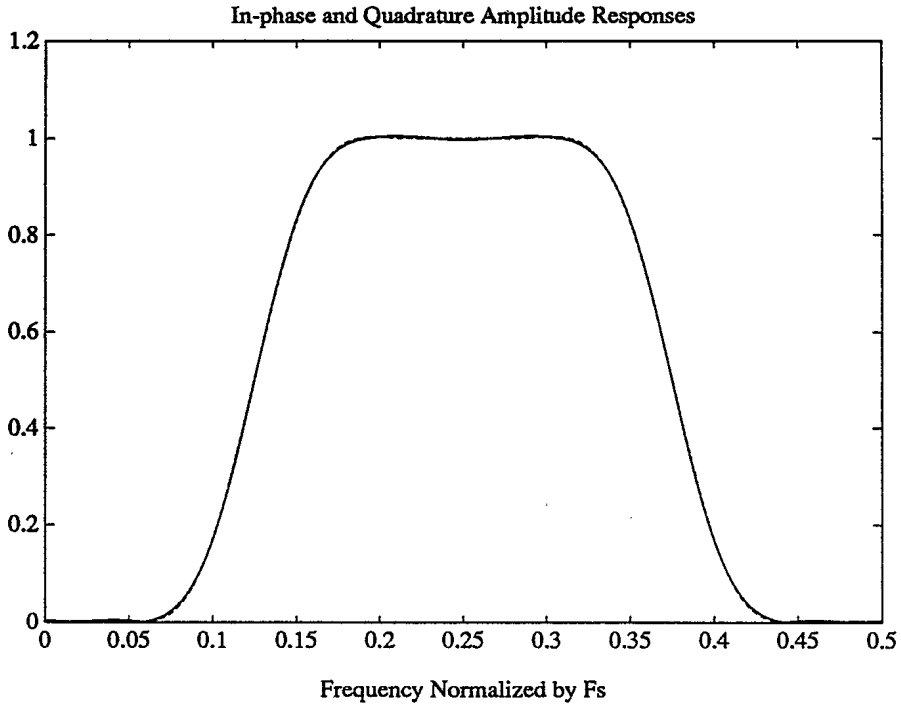

Figure 25: Matched amplitude responses for 29 tap filters.

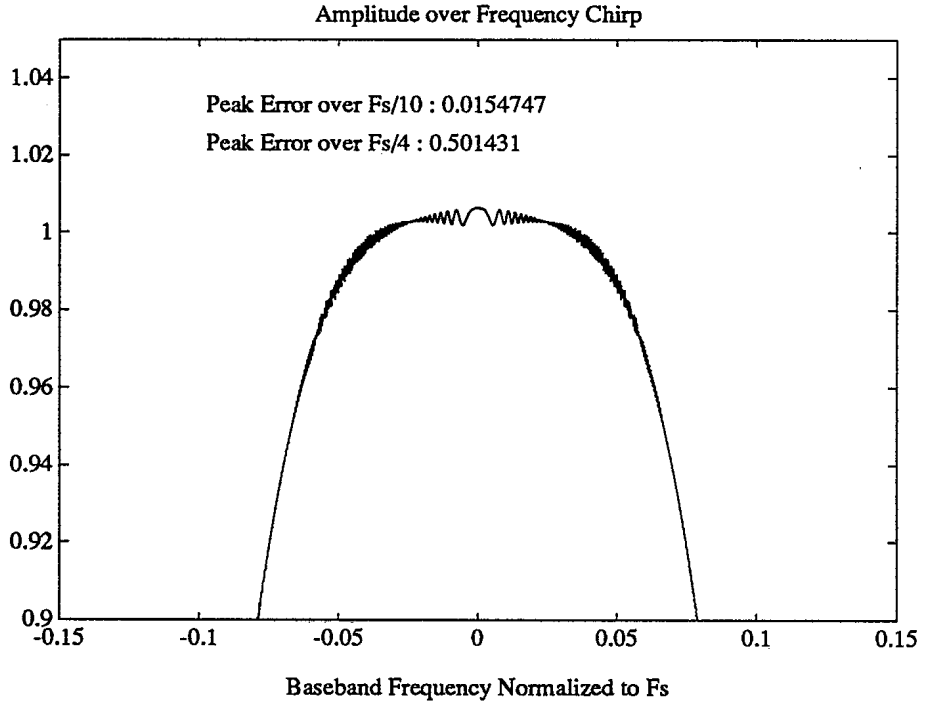

Figure 26: Amplitude results for chirp test of 21 tap Matched Response demodulator.

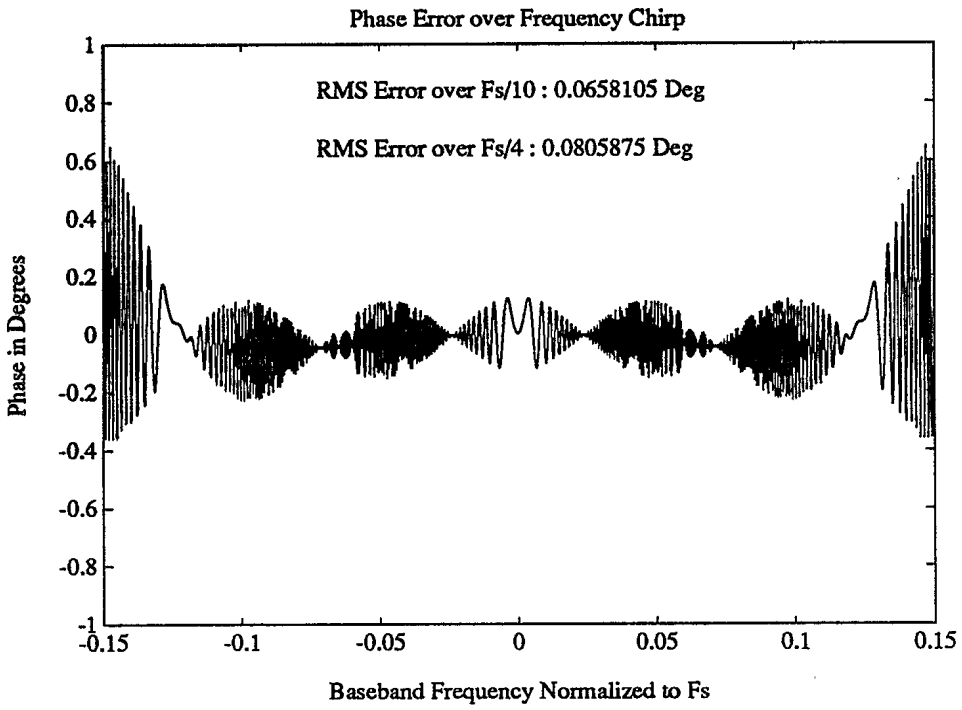

Figure 27: Phase results for chirp test of 21 tap Matched Response demodulator.

with the effects of quantization of both coefficients and sampling rolled into the results. Although results were compiled for all three of the trapezoidal, Gaussian and raised cosine pulses, only results from one trapezoidal pulse and one raised cosine pulse are shown for the sake of brevity.

Fig. 29 shows the ideal and obtained demodulator output amplitude for a trapezoidal one microsecond width pulse with 100 nanosecond rise and fall times. The ideal sample values are marked by '+' characters and the obtained values are marked by 'o' characters. The sampling rate for this and other experiments was set at 400 MHz, thereby making the IF 100 MHz. The initial frequency is 95 MHz (5 Mhz below the IF), and a linear frequency modulation of 10 MHz per microsecond is used.

Fig. 30 shows the complex valued error at the demodulator output. The error is at all times less than 1% of the pulse amplitude, a very impressive performance.

Fig. 31 shows the magnitude of the error at the demodulator output over time. The largest errors occur at the leading and trailing edges of the pulse, where the demodulator filter transients appear.

Fig. 32 shows the phase error (the difference in demodulator output phase from the ideal output phase) over time. Only the output samples where the output magnitude

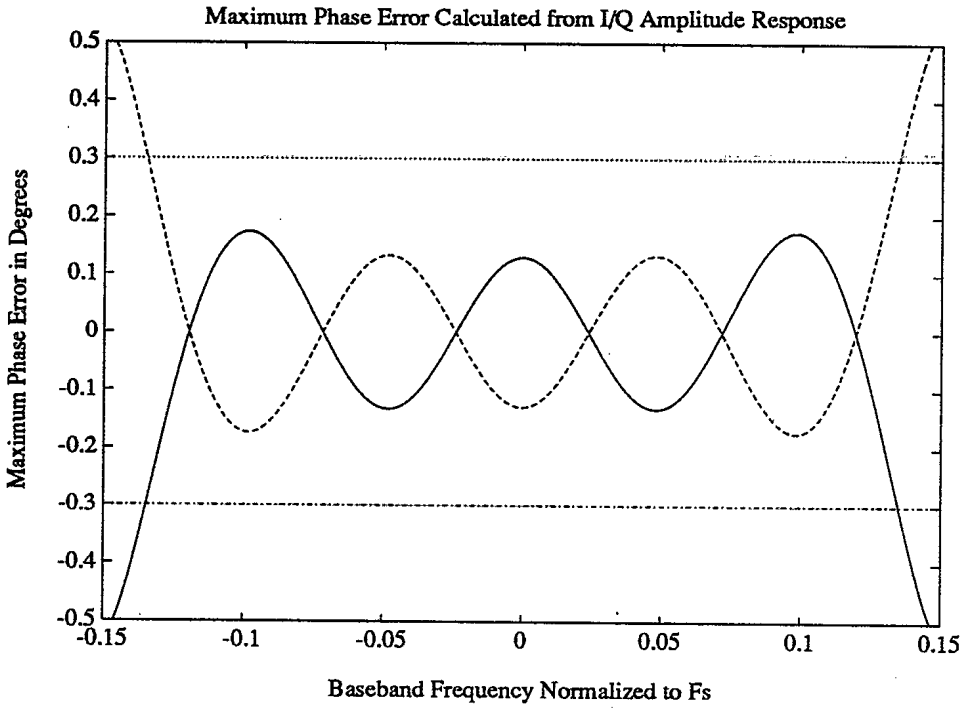

Figure 28: Phase error bounds for 21 tap Matched Response demodulator. The horizontal lines indicate the 0.3° phase error design goal.

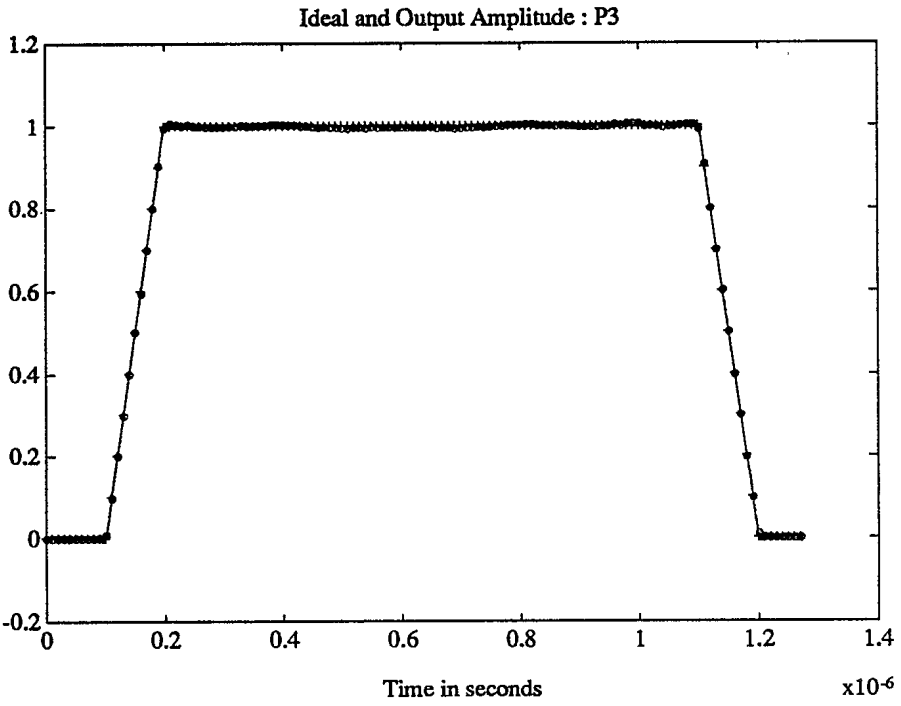

Figure 29: Amplitude for ideal and obtained demodulator output, 1 microsecond trapezoidal pulse.

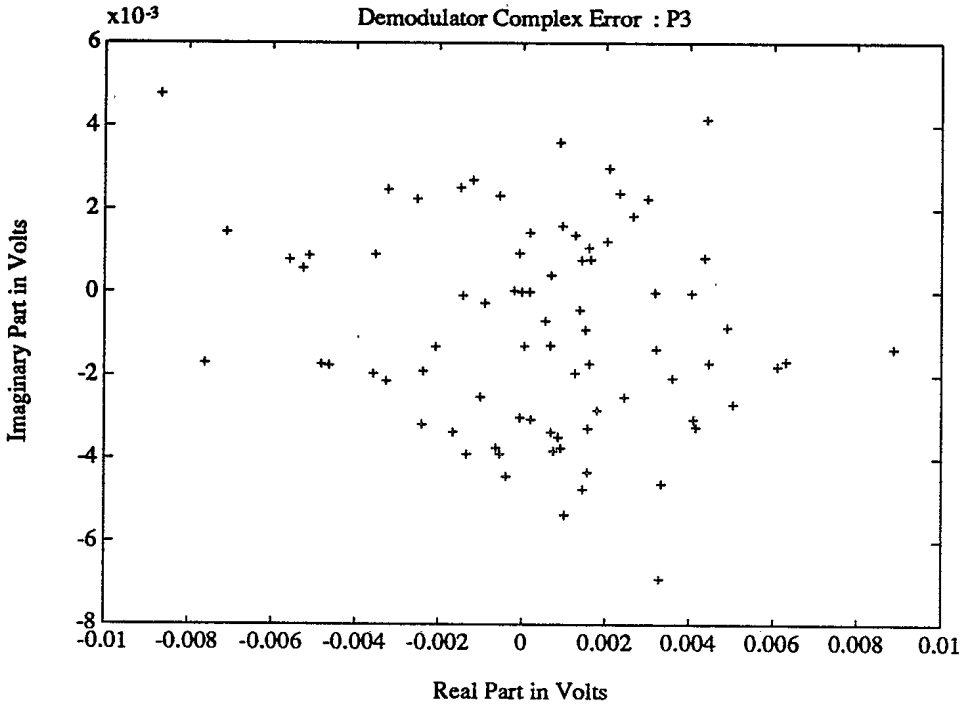

Figure 30: Complex error, 1 microsecond trapezoidal pulse.

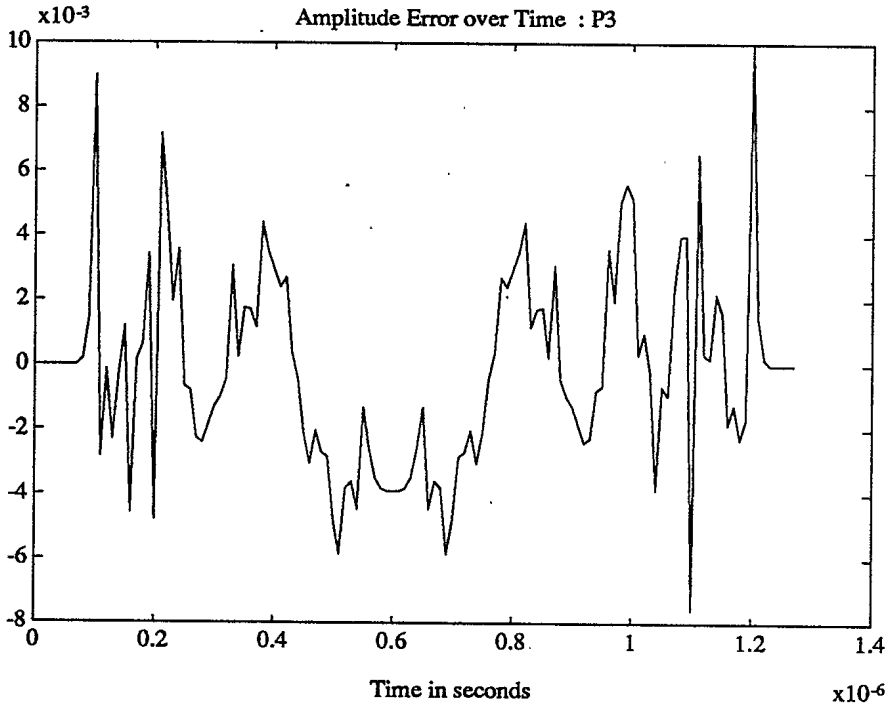

Figure 31: Amplitude of errors over time, 1 microsecond trapezoidal pulse.

of the complex pair is greater than 5% of the maximum pulse amplitude are considered in the figure. This thresholding allows us to screen out the phase values corresponding to low amplitude output values and is desirable because the tails of the filtered pulse waveform have little information content due to quantization errors and the aliasing resulting from the infinitely wide spectrum of a time-limited pulse waveform. The phase errors are *typically* below 0.3°, but approach 1° at the pulse edges, where the filter transients occur. The phase error comes within the 0.3° design goal about halfway through the rise time interval.

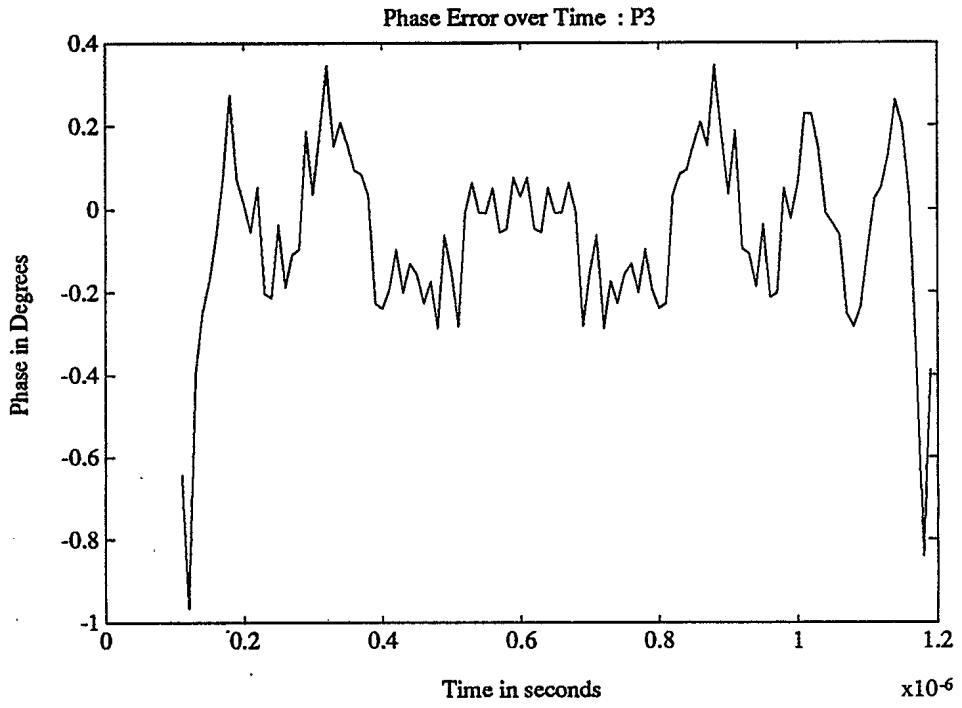

Figure 32: Significant phase errors over time, 1 microsecond trapezoidal pulse.

Fig. 33 shows the ideal and obtained demodulator output amplitude for a 500 nanosecond width pulse with raised cosine edges and 50 nanosecond rise and fall times. The initial frequency is 110 MHz (10 Mhz above the IF), and no frequency modulation is used.

Fig. 34 shows the complex valued error at the demodulator output. The error is at all times less than 1% of the pulse amplitude, again a very impressive performance.

Fig. 35 shows the magnitude of the error at the demodulator output over time. The largest errors occur at the leading and trailing edges of the pulse, where the demodulator filter transients appear.

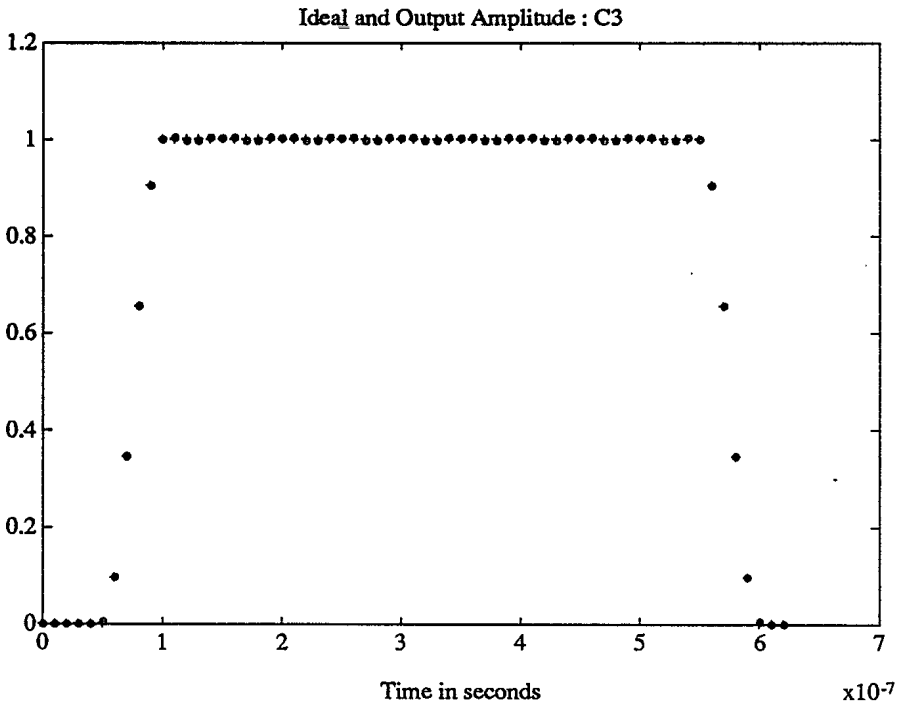

Figure 33: Ideal and obtained demodulator output, 500 nanosecond cosine-edged pulse.

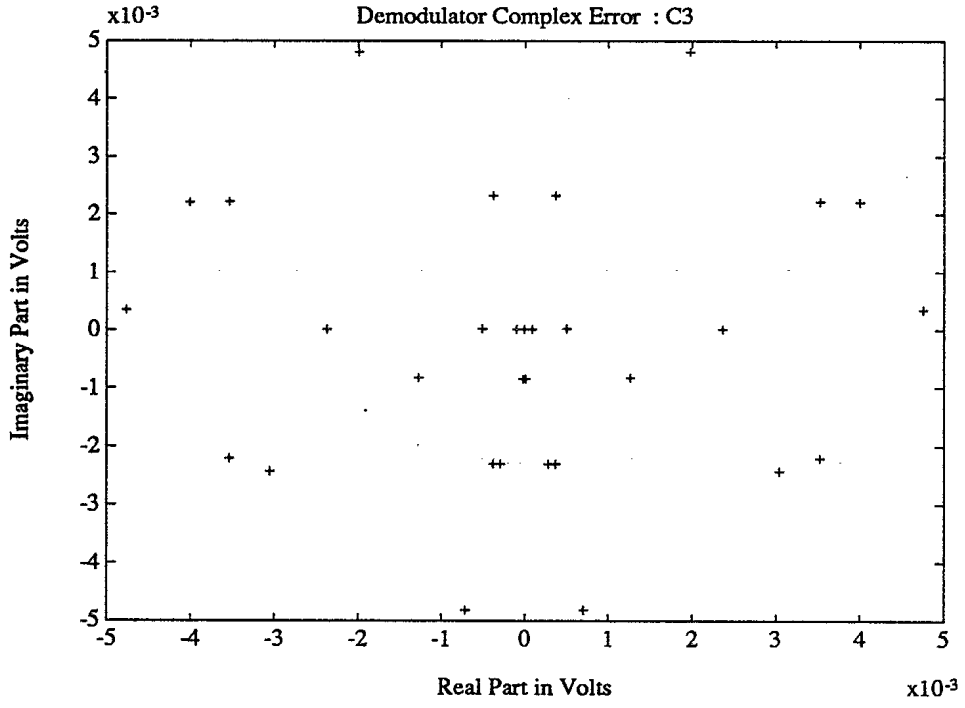

Figure 34: Complex error, 500 nanosecond cosine-edged pulse.

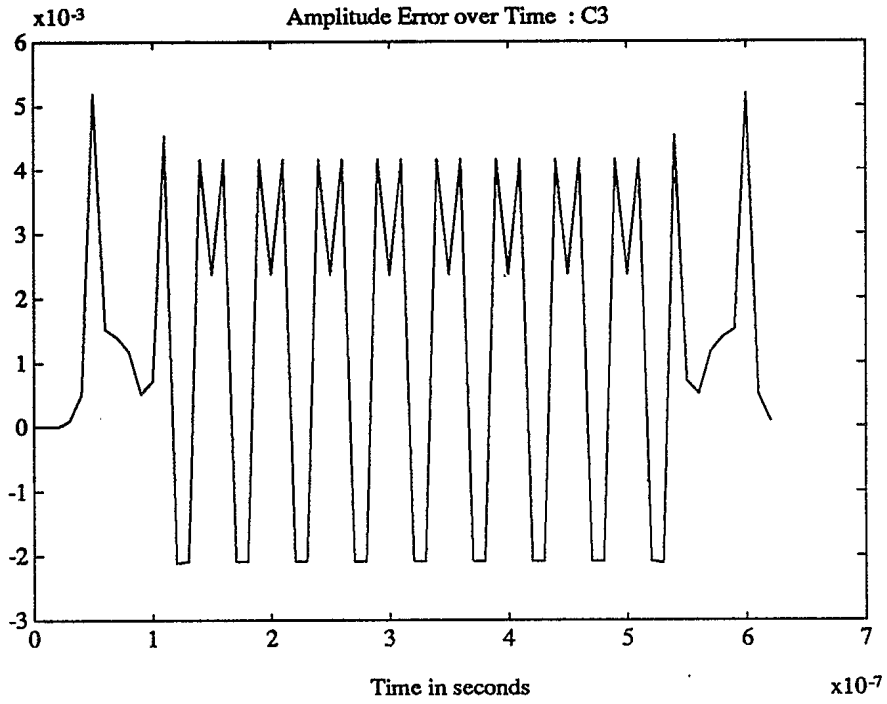

Figure 35: Amplitude of errors over time, 500 nanosecond cosine-edged pulse.

Fig. 36 shows the phase error (the difference in demodulator output phase from the ideal output phase) over time. Only the output samples where the output magnitude of the complex pair is greater than 5% of the maximum pulse amplitude are considered. The phase errors are *typically* below 0.3°, but approach 0.6° at the pulse edges. The phase error comes within the 0.3° design goal about halfway through the rise time interval.

These results are respresentative of the overall body of tests which showed that the Wide Bandwidth Matched Response design performed very well with pulse signals. Given a requirement for a zero DC offset design, the Matched Response design is a good candidate for use in a practical RESM system.

If it can be shown that DC offsets introduced by the A/D converter may be controlled outside of the demodulator, the Medium Bandwidth Simple Hilbert Transformer design might be favoured because of its extreme simplicity.

The Medium Bandwidth, zero offset design could be considered if DC offset removal is a requirement, if moderate bandwidth is acceptable, and if the additional complexity of the Matched Response design can be achieved only at significant cost.

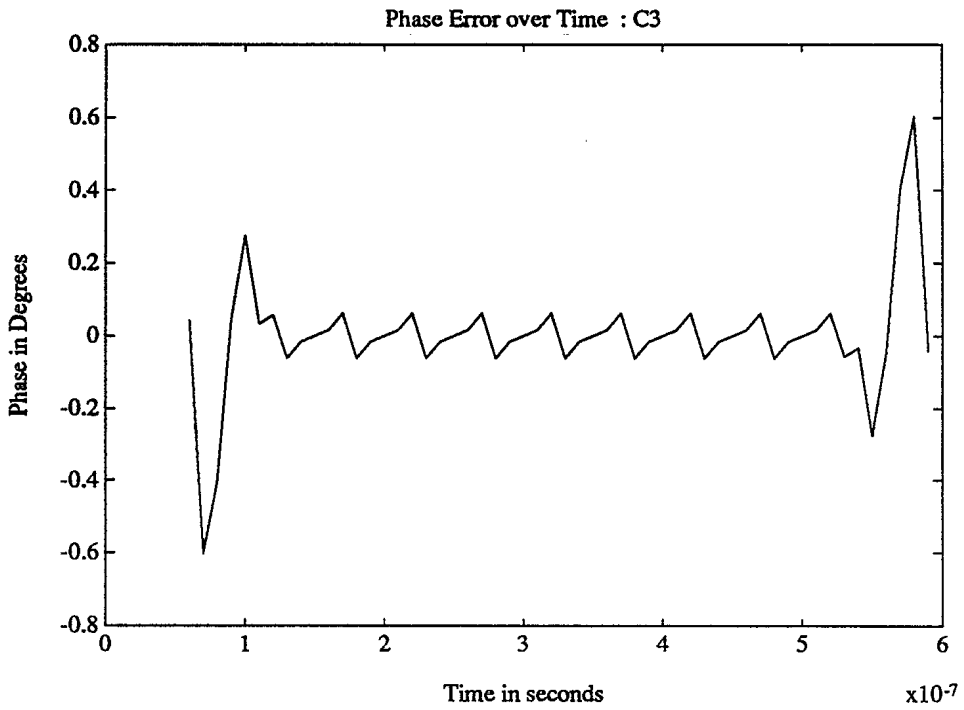

Figure 36: Significant phase errors over time, 500 nanosecond cosine-edged pulse.

3.0 CONCLUSION

Technology advances in microelectronics and analog-to-digital converters facilitate the implementation of wideband, real-time, coherent quadrature demodulators using digital techniques. This report shows that with careful design relatively simple filters can be used to achieve a very good performance suitable for advanced radar and RESM applications.

Given the further advantages of application specific circuits in terms of manufacturing cost, reliability, power consumption, size and weight, it is anticipated that the implementation of digital quadrature demodulation and other signal processing functions by application specific integrated circuits will be an important aspect of future RESM and radar systems.

ACKNOWLEDGEMENTS

The authors acknowledge the assistance of Serge Martineau of Applied Silicon Inc. Canada in the course of this work. Mr Martineau provided support in the form of software to generate pulse waveforms, useful discussion, and guidance in the use of computer tools. They also acknowledge the important contribution of Dr J.P.Y. Lee of the Defence Research Establishment Ottawa to the analysis presented in Appendix A.

APPENDIX

A.0 THE EFFECTS OF I/Q AMPLITUDE MISMATCH

Any bandpass signal $r(t)$ may be represented as:

$$\begin{aligned} r(t) &= A(t)\cos[\omega_o t + \phi(t)] && \text{(A.1)} \\ &= A(t)\cos\phi(t)\cos\omega_o t \; - \; A(t)\sin\phi(t)\sin\omega_o t && \text{(A.2)} \\ &= I(t)\cos\omega_o t \; - \; Q(t)\sin\omega_o t. && \text{(A.3)} \end{aligned}$$

where $I(t) = A(t)\cos\phi(t)$, $Q(t) = A(t)\sin\phi(t)$, and ω_o is the carrier frequency in radians per second.

In our case we use finite impulse response filters to obtain estimates of the in-phase and quadrature components. For both digital and analog implementations the in-phase and quadrature component estimates are affected by frequency dependent mismatches in the gain of the two channels which can be represented by the gain factors $K_i(\omega)$ and $K_q(\omega)$ respectively:

$$\begin{aligned} \hat{I}(t) &= K_i(\omega)A(t)\cos\phi(t) && \text{(A.4)} \\ \hat{Q}(t) &= K_q(\omega)A(t)\sin\phi(t) && \text{(A.5)} \end{aligned}$$

The measured phase (which is an estimate of $\phi(t)$) is given by:

$$\begin{aligned} \theta(t) &= \tan^{-1}\left[\frac{K_i(\omega)A(t)\cos\phi(t)}{K_q(\omega)A(t)\sin\phi(t)}\right] && \text{(A.6)} \\ &= \tan^{-1}\left[R\ \tan\phi(t)\right] && \text{(A.7)} \end{aligned}$$

where $R = K_i(\omega)/K_q(\omega)$, and tan is the four-quadrant tangent. The phase error, ϵ, is therefore:

$$\epsilon(t) = \theta(t) - \phi(t) = \tan^{-1}\left[R\tan\phi(t)\right] - \phi(t) \qquad \text{(A.8)}$$

We can see that the phase error is a function of $\phi(t)$, the time-varying phase of the modulating signal being measured. The parameter R determines the severity of

APPENDIX

the phase distortions around the unit circle, with a value of 1 (no amplitude imbalance) leading to zero phase distortion. To simplify notation, we can drop the time argument and simply write:

$$\epsilon(\phi) \;=\; \tan^{-1}\left[R\tan\phi\right] \;-\; \phi \tag{A.9}$$

for all time. The error ϵ depends upon the actual phase ϕ. By taking the derivative and setting it to zero we find that the maximum error occurs at ϕ_{max} where:

$$\phi_{max} \;=\; \cos^{-1}\left(\sqrt{\frac{R}{1+R}}\right) \tag{A.10}$$

Replacing ϕ by ϕ_{max} in equation A.9 gives

$$\epsilon_{max} \;=\; \tan^{-1}\left[R\tan\phi_{max}\right] \;-\; \phi_{max} \tag{A.11}$$

If we make the approximation that $\sqrt{R/(1+R)} \;\approx\; \frac{1}{\sqrt{2}}$ for $R \approx 1$, then we have:

$$\epsilon_{max} \;\approx\; \tan^{-1} R \;-\; \frac{\pi}{4} \tag{A.12}$$

This last approximate expression was used in sections 2.4.2 and 2.5 to compute the maximum phase error bounds given the amplitude responses of the in-phase and quadrature filters. The ratio of the amplitude responses at each frequency maps to a valid value of ϵ_{max} at that frequency.

Fig. 37 shows plots of the actual and approximate functions for ϵ_{max}, demonstrating the accuracy of the approximation over a very wide range of imbalances. Over the very small imbalances we are designing for (less than 1%), the approximation is virtually perfect.

Since R is frequency dependent and may be obtained from the amplitude response of the FIR filters in our case, the appropriate values of R and $|\epsilon_{max}|$ may be found for all frequencies. The amplitude responses are, in turn, easily obtained from the FIR filter coefficients alone.

APPENDIX

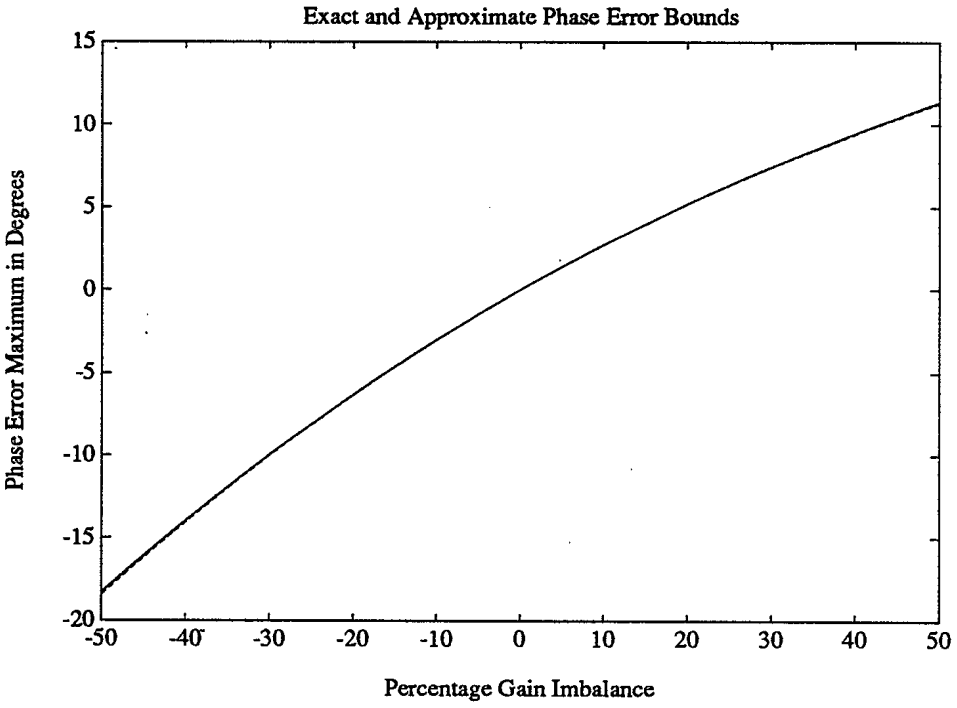

Figure 37: Actual vs. approximate values for ϵ_{max}.

REFERENCES

[1] R. V. Blerkom, D. G. Freeman, and R. C. Crutchfield, "Frequency measurement techniques," *IEEE Transactions Instrum. and Meas.*, vol. 17, no. 2, pp. 12–20, June 1968.

[2] M. I. Skolnik, *Radar Handbook, 2nd Edition.* McGraw-Hill, 1990.

[3] J. M. Dunn-Rogers, "Digital sampling techniques for ESM receivers," in *Proceedings of the 1990 Military Microwave Conference*, 1990.

[4] R. J. Inkol, *Algorithms for the Direct Comparison of Intrapulse Signal Data.* DREO Technical Memorandum 21/91, 1991.

[5] F. E. Churchill, G. W. Ogar, and B. J. Thompson, "The correction of I and Q errors in a coherent processor," *IEEE Trans. Aerosp. and Electron. Syst.*, vol. 17, no. 1, Jan. 1981.

[6] J. P. Y. Lee, "Quadrature sampling for radar ESM applications," in *CRAD Signal Processing Symposium*, 1991.

[7] J. van Valburg and R. van de Plassche, "An 8b 650 mhz folding adc," in *Proceedings of the International Solid State Circuits Conference*, Feb. 1992.

[8] W. M. Waters and B. R. Jarret, "Bandpass signal sampling and coherent detection," *IEEE Trans. Aerosp. and Electron. Syst.*, vol. 18, no. 4, pp. 731–736, Nov. 1982.

[9] T. Thiel and G. Saulnier, "Simplified complex digital sampling demodulator," *Electron. Letters*, vol. 26, no. 7, pp. 419–421, Mar. 1990.

[10] G. Rempel and G. Haslam, "A digital demodulation scheme for use in a high dynamic range radar system," in *Proceedings of Canadian Conference on Computer and Electrical Engineering*, pp. 419–421, Sept. 1991.

[11] E. April, *Comparison of Digital Spectral Shifters.* DREO Technical Memorandum 25/90, 1990.

[12] R. L. Mitchell, "Creating complex signal samples from a band-limited real signal," *IEEE Trans. Aerosp. and Electron. Syst.*, vol. 25, no. 3, pp. 425–427, May 1989.

REFERENCES

[13] D. Roy and R. Inkol, "A high-accuracy digital coherent detector," in *Proceedings of the Thirteenth Biennial Symposium on Communications*, June 1986.

[14] J. H. Lodge, "Private communication," *Communications Research Centre, Department of Communications, Canada.*

[15] L. R. Rabiner and B. Gold, *Theory and Application of Digital Signal Processing.* Prentice-Hall, 1975.

[16] D. J. Goodman and M. J. Carey, "Nine digital filters for decimation and interpolation," *IEEE Trans. ASSP*, vol. 25, no. 2, pp. 121–126, Apr. 1977.

DOCUMENT CONTROL DATA

(Security classification of title, body of abstract and indexing annotation must be entered when the overall document is classified)

1. ORIGINATOR (the name and address of the organization preparing the document. Organizations for whom the document was prepared, e.g. Establishment sponsoring a contractor's report, or tasking agency, are entered in section 8.)

NATIONAL DEFENCE
DEFENCE RESEARCH ESTABLISHMENT OTTAWA
SHIRLEY BAY, OTTAWA, ONTARIO K1A 0K2 CANADA

2. SECURITY CLASSIFICATION (overall security classification of the document. including special warning terms if applicable)

UNCLASSIFIED

3. TITLE (the complete document title as indicated on the title page. Its classification should be indicated by the appropriate abbreviation (S,C or U) in parentheses after the title.)

DIGITAL QUADRATURE DEMODUALTION FOR RADAR ESM APPLICATIONS (U)

4. AUTHORS (Last name, first name, middle initial)

INKOL, ROBERT
SAPER, RON

5. DATE OF PUBLICATION (month and year of publication of document)	6a. NO. OF PAGES (total containing information. Include Annexes, Appendices, etc.)	6b. NO. OF REFS (total cited in document)
MAY 1992	48	19

7. DESCRIPTIVE NOTES (the category of the document, e.g. technical report, technical note or memorandum. If appropriate, enter the type of report, e.g. interim, progress, summary, annual or final. Give the inclusive dates when a specific reporting period is covered.)

DREO TECHNICAL NOTE

8. SPONSORING ACTIVITY (the name of the department project office or laboratory sponsoring the research and development. Include the address.)

NATIONAL DEFENCE
DEFENCE RESEARCH ESTABLISHMENT OTTAWA
~~SHIRLEY BAY, OTTAWA, ONTARIO K1A 0K2 CANADA~~

9a. PROJECT OR GRANT NO. (if appropriate, the applicable research and development project or grant number under which the document was written. Please specify whether project or grant)	9b. CONTRACT NO. (if appropriate, the applicable number under which the document was written)
011LB11	W7714-1-9993

10a. ORIGINATOR'S DOCUMENT NUMBER (the official document number by which the document is identified by the originating activity. This number must be unique to this document.)	10b. OTHER DOCUMENT NOS. (Any other numbers which may be assigned this document either by the originator or by the sponsor)
DREO TECHNICAL NOTE 92-10	

11. DOCUMENT AVAILABILITY (any limitations on further dissemination of the document, other than those imposed by security classification)

(X) Unlimited distribution
( ) Distribution limited to defence departments and defence contractors; further distribution only as approved
( ) Distribution limited to defence departments and Canadian defence contractors; further distribution only as approved
( ) Distribution limited to government departments and agencies; further distribution only as approved
( ) Distribution limited to defence departments; further distribution only as approved
( ) Other (please specify):

12. DOCUMENT ANNOUNCEMENT (any limitation to the bibliographic announcement of this document. This will normally correspond to the Document Availabilty (11). However, where further distribution (beyond the audience specified in 11) is possible, a wider announcement audience may be selected.)

UNCLASSIFIED

SECURITY CLASSIFICATION OF FORM

13. ABSTRACT (a brief and factual summary of the document. It may also appear elsewhere in the body of the document itself. It is highly desirable that the abstract of classified documents be unclassified. Each paragraph of the abstract shall begin with an indication of the security classification of the information in the paragraph (unless the document itself is unclassified) represented as (S), (C), or (U). It is not necessary to include here abstracts in both offical languages unless the text is bilingual).

(U) Techniques for digital in-phase and quadrature demodulation are investigated for application in Radar Electronic Support Measures (RESM) systems.

14. KEYWORDS, DESCRIPTORS or IDENTIFIERS (technically meaningful terms or short phrases that characterize a document and could be helpful in cataloguing the document. They should be selected so that no security classification is required. Identifiers, such as equipment model designation, trade name, military project code name, geographic location may also be included. If possible keywords should be selected from a published thesaurus. e.g. Thesaurus of Engineering and Scientific Terms (TEST) and that thesaurus-identified. If it is not possible to select indexing terms which are Unclassified, the classification of each should be indicated as with the title.)

DIGITAL SIGNAL PROCESSING
COHERENT DEMODULATION
QUADRATURE DEMODULATION
FINITE IMPULSE RESPONSE FILTER

93-00059

NO. OF COPIES NOMBRE DE COPIES	COPY NO. COPIE N°	INFORMATION SCIENTIST'S INITIALS INITIALES DE L'AGENT D'INFORMATION SCIENTIFIQUE
1	1	JAN 21 DAG

AQUISITION ROUTE FOURNI PAR ▶	DREO
DATE ▶	23 DECEMBER 1992
DSIS ACCESSION NO. NUMÉRO DSIS ▶	93-00059

DND 1158 (6-87)

National Defence / Défense nationale

#127314